

# On two-dimensional foam ageing

J. DUPLAT<sup>1</sup>, B. BOSSA<sup>2</sup> AND E. VILLERMAUX<sup>3†</sup>

<sup>1</sup>Aix-Marseille Université, IUSTI, 13453 Marseille Cedex 13, France

<sup>2</sup>Aix-Marseille Université, IRPHE, 13384 Marseille Cedex 13, France

<sup>3</sup>Institut Universitaire de France, 103, boulevard Saint-Michel, 75005 Paris, France

(Received 16 December 2009; revised 27 July 2010; accepted 30 November 2010)

The present study aims at documenting, making use of an original set-up allowing to acquire well-converged data, the coarsening of foams in two dimensions. Experiments show that a foam behaves quite differently depending on the way it has been prepared. We distinguish between an initially quasi-monodisperse foam and a polydisperse foam. The coarsening laws are initially different, although both foams reach a common, time-dependent asymptotic regime.

The ageing process relies on exchanges between adjacent foam cells (von Neumann's law), and on topological rearrangement ( $\mathcal{T}_1$  and  $\mathcal{T}_2$  processes) whose rates are measured in all regimes. We attempt to make their contribution to the evolution of the area  $S$  and facet number  $n$  distribution of probability  $P(S, n, t)$  quantitative. The corresponding mean field theory predictions represent well the phenomenon qualitatively, and are sometimes in quantitative agreement with the measurements. A simplified version of this theory, taking the form of a Langevin model, explains in a straightforward manner the different scaling laws in the different regimes, for the different foams.

**Key words:** capillary flows, complex fluids, foams

---

## 1. Introduction

Two-dimensional soap froth is a representative case of a broad class of problems consisting in covering the plane by contiguous sub-areas, or cells. Albeit trivial solutions exist (mapping the plane by regular shapes like squares, or hexagons for instance), it is frequently observed in several physical and natural systems that a disordered solution is adopted. For a medium evolving in time with growing cells, as for biologic tissues, it is not possible to maintain a perfect lattice, and the medium becomes disordered. The cell features (their area, their number of facets) are distributed, all the more broadly as if the systems have aged. General properties appear to hold for several different systems, which are subjected to identical geometrical and topological constraints (Mombach, de Almeida & Iglesias 1993; Stavans 1993; Weaire & Hutzler 1999). Among them is Lewis Law, first established for human retina epithelium and for cucumber rind (Lewis 1928). It expresses the existence of a correlation between the area and the number of facets of a single cell. Another common feature of these systems is the time dependence of the average cell radius  $\langle r(t) \rangle$ . It is observed that  $\langle r(t) \rangle \propto t^{1/2}$ , holding for grain growth (Cleri 2000), or in soap

† Email address for correspondence: villermaux@irphe.univ-mrs.fr

froth system (Tam & Szeto 1996) both in two and three dimensions (at the notable exception of accreted ice domains which present a much weaker time dependence, see, e.g. Prodi & Levi 1980).

The present work concerns the classical problem of ageing of two-dimensional dry soap froths. A foam is continuously formed at the entrance of a channel, through which it is progressively transported (§2.1). The foam ages as it travels through the channel. Each downstream position in the channel corresponds to a given age of the foam, thus allowing to reconstruct its history. As we obtain a steady, permanently regenerated system, large amounts of data are easily collected allowing, after appropriate processing to compute high-quality statistics on various aspects of the cells constitutive of the foam (§2.2).

Two different regimes are observed, corresponding to different injection conditions. For a polydisperse foam (run **P**), our observation for the evolution of average area  $\langle S \rangle$  recovers the results already observed and one has  $\langle S \rangle \sim t$ . In this regime, the distribution of surfaces  $P(S, t)$  is shown to evolve self-similarly in time  $t$  leading to a stationary distribution  $P(S/\langle S \rangle)$ , as also observed by others (Stavans 1990; Segel *et al.* 1993; de Icaza, Jimenez Cenicerros & Castano 1994). The large statistics accumulated in our experiment allow the measurements of the distribution  $P(S, n, t)$  of the cell surfaces  $S$  conditioned to their facet number  $n$ , and in particular the first moment  $\langle S|n \rangle$  and second moment  $\sigma_n^2$  of this distribution. If several authors (Glazier, Gross & Stavans 1987; Szeto & Tam 1995) have reported about the so-called Lewis law ( $\langle S|n \rangle \propto n$ ), observations for the second moment are new.

For an initially monodisperse foam (run **M**), the same measurements are made, and a new regime is observed: the typical cell area grows like  $t^{3/2}$ . In this case, the evolution of the distribution  $P(S, n, t)$  is not self-similar. On the contrary, we show that this new regime is a transient evolution toward the final self-similar regime. The distribution of the number of cell facets  $P(n)$  evolves from a Dirac distribution  $P(n) = \delta_{n,6}$  at initial time toward a stationary distribution, exhibiting an exponential shape, a classical behaviour for two-dimensional cellular structures (Miri & Rivier 2006). The distribution  $P(n)$  obtained with this initially monodisperse foam is particularly broad (cells with up to  $n = 15$  facets are observed with statistical significance). This observation, made possible thanks to the large amount of statistics, singles out a regime where the  $\mathcal{T}_1$  topological processes are frequent.

Since the cells are tracked in time, we also obtain the temporal evolution of the properties of each individual cell. The elementary processes ruling the evolution of the foam are known. In a soap froth, gas exchange happens between cells, as a consequence of pressure differences, themselves related to the cells topology. The latter depends simply (for a two-dimensional froth) on the number of facets of a given cell (von Neumann 1952 and §4.1). Concomitantly, the local structure of the foam is modified through so-called  $\mathcal{T}_1$  and  $\mathcal{T}_2$  topological processes, which lead to a modification of the number of facets  $n$ . We quantify these phenomena, measuring the gas exchange rate  $\dot{S}^*$  of von Neumann's law, and the rates  $\beta$  and  $\alpha$  of the topological processes (§4.2). Our measurement technique allow us to characterize *quantitatively* these processes: the gas exchange rate  $\dot{S}^*$  of von Neumann's law is measured, the frequency of topological processes is measured and is shown to be related with the cell's facet number  $n$ .

These quantitative descriptions of the evolution of individual cells allow us to discuss an analytical model based on a mean field approach in the spirit of the one imagined by Flyvbjerg (1993) for the evolution of the cell area  $S$  and facet number  $n$  distribution  $P(S, n, t)$  as a function of time  $t$ , based on our experimental observations.

In contrast with other approaches using a lumped parameterization of the cell's rate of growth conditioned to their radius (Beenakker 1986; Streitenberger & Zollner 2006) or of the cell facet number variations (Marder 1987), we make the effect of the topological processes explicit in that formulation, and derive analytical predictions for the mean and variance of the area distribution, in particular (§ 5.1). The same principles rule the evolution of the transient (run *M*) and self-similar (run *P*) regimes which are both predicted within the same theoretical framework.

Finally, we suggest in § 6 that ageing in foams can be understood from a simple Langevin model, which retains the essential ingredients of our more elaborate description, and for which we identify the origin of the damping term, and of the random forcing in relation with the topological changes within the foam. This model provides a transparent explanation for the existence of two coarsening regimes, Lewis law, and the growth of the cell's average surface.

## 2. Set-up and image processing

### 2.1. The foam channel

The foam is formed from bubbles injected into a layer of soapy solution at the entrance of a long channel. The solution is made from a commercial surfactant (Dreft by Procter & Gamble, a mixture of non-ionic and anionic molecules) diluted into tap water offering a static surface tension (measured using the protocol of Hansen & Rodsrud 1991) of  $\gamma = 32 \times 10^{-3} \text{ N m}^{-1}$ .

The channel is 0.7 mm thick, 20 cm wide, and 2 m long (figure 1). It is made of two parallel thick (1 cm) glass plates which are rigid enough to ensure that the inner gap of the channel is uniform. This set-up allows a direct visualization of the foam by transparency. The whole channel is tilted at an angle of about  $20^\circ$  with the horizontal, keeping a reservoir of soapy water filling the lowest 20 cm of the channel (figure 2). The other extremity of the channel is opened to the atmosphere.

Carbon dioxide ( $\text{CO}_2$ ) gas, chosen for its high solubility in water, is discharged at the bottom of the channel through a 100- $\mu\text{m}$ -diameter needle dipping in the soapy water layer. Bubbles of typically  $4 \text{ mm}^3$  are formed in the neighbourhood of the needle exit and since the channel is thin enough, the corresponding gas volume is squeezed in the gap between the plates so that the bubbles are quasi two-dimensional. Bubbles rise from the injection point, through the soapy water and collect at the solution/air interface, packing and forming a foam above the soapy water as seen in figure 2.

A monodispersed foam is built by producing regular bubbles (all with the same volume), whereas a polydispersed foam results from more random bubble sizes generating conditions at the needle nozzle, which soon prevail when the gas flow rate is increased through the needle. In both cases, the bubbles settle toward the interface, aggregate and rearrange in the foam. The rearrangements are not controlled, but in the case of a monodispersed collection of bubbles, it is observed that a nearly regular hexagonal lattice is formed. In the polydispersed case, no regular structure is observed (figure 3).

The arrival of new bubbles at the bottom of the foam induces a very slow flow, pushing the whole foam toward the exit point at the other extremity of the channel. The pre-wetting of the channel walls reduces the friction of the foam on the walls and no pinning is observed. This ensures that the foam ageing process will not be hindered by the existence of pinning points which would otherwise cause a freezing of the evolution, known to occur as soon as the average cell radius is equal to the distance between pinning spots (Krichevsky & Stavans 1992).

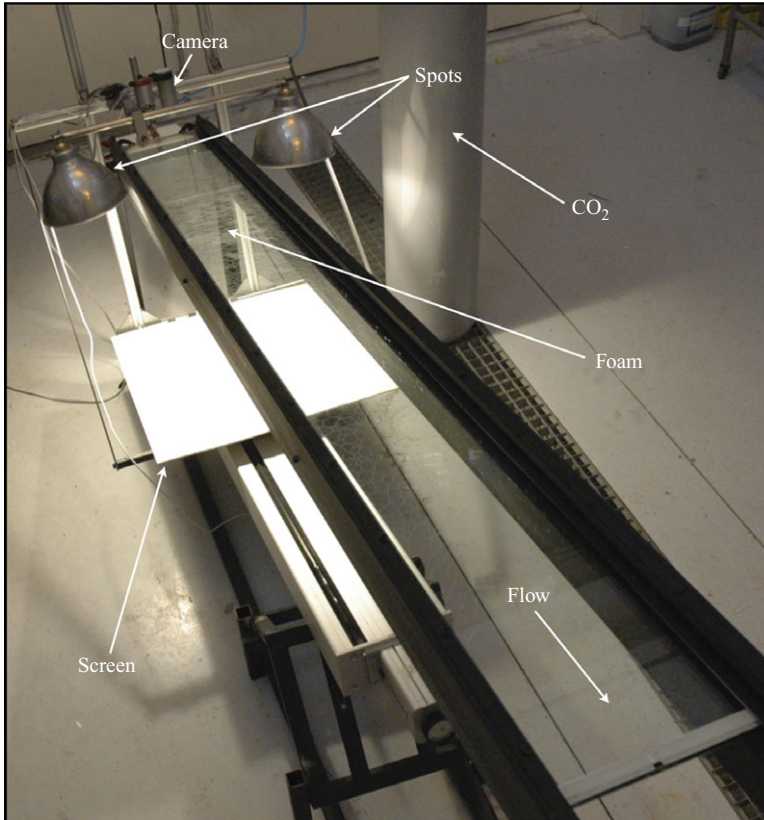


FIGURE 1. (Colour online available at [journals.cambridge.org/FLM](http://journals.cambridge.org/FLM)) Overview of the foam channel. The foam is sandwiched between two thick glass plates and is visualized by transparency with a white screen lightened by two spots embarked, with the camera, on a trolley travelling along the channel as the foam flows through it.

Foam is known to be a typical multiphase media with a non-Newtonian rheology (Cantat, Kern & Delannay 2004; Hilgenfeldt, Arif & Tsai 2008). The foam rheological behaviour is determined by the dominant dissipation mechanism, namely the sliding of plateau borders over the channel walls. When the foam moves, the strain thus applies on a very thin layer at the border of the channel. Thus, side cells slip at the border of the channel at a velocity close to the flow velocity. Consequently, the average velocity profile of the foam across the channel width is a quasi-perfect plug flow. The fluctuations of velocity due to the local rearrangement dynamics as the foam coarsens are weak, of the order of 3% of the average drift velocity  $U_T$ .

This configuration, where the foam is permanently renewed and coarsened in steady state as it travels through the channel, was chosen on purpose, because it allows to collect easily a large amount of statistics. The correspondence between the position  $z$  of an element of foam in the channel and the time  $t$  it has spent in the channel to reach this position is

$$z = U_T t, \quad (2.1)$$

where  $U_T$  is the mean drift velocity. Equation (2.1) is known in the context of turbulence as ‘Taylor relationship’ that is frequently used for relating space to time in

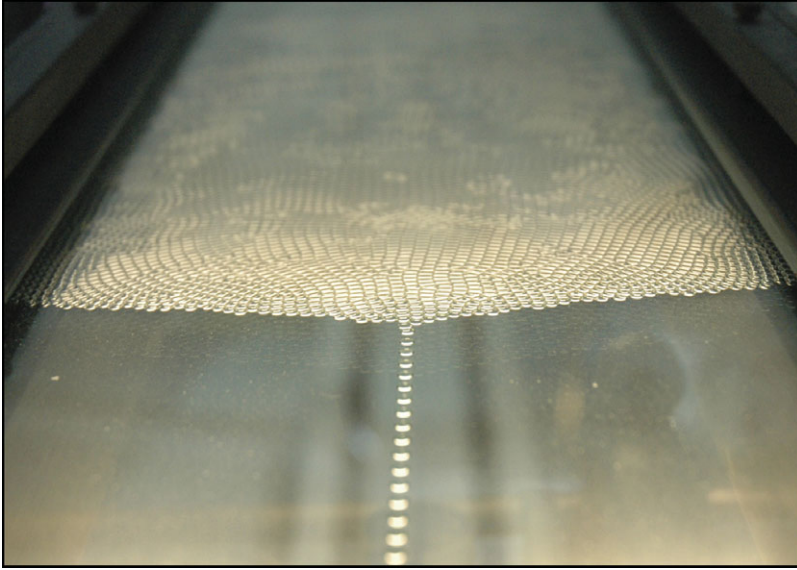


FIGURE 2. (Colour online) Detail of the bubble injection mechanism. The  $\text{CO}_2$  bubbles are formed from a needle dipping into the soap solution.

weakly fluctuating media, as in wind tunnels for instance. Averages and distributions for a given age  $t$  are then calculated at a given position  $z$  and in the following, we will refer to the age  $t$  of the foam. In this respect, our channel is a ‘foam tunnel’.

### 2.2. Image capture and reconstruction

In order to obtain significant and reliable statistics, a large number of images of the foam as it ages are captured in the following way: the foam channel is 2 m long, and a single cell has a typical diameter of a few millimetres; the separatrix between the cells is even smaller (the visible separatrix foot at the channel wall is typically 0.5 mm thick). We thus perform a scan of the foam. Making use of a commercial webcam (Apple iSight) of standard PAL resolution ( $640 \times 480$  pixels), a snapshot of the foam is realized covering the total width of the channel (i.e., 20 cm) and only a small subpart of its length (i.e., 15 cm) to ensure the locality of the measurement. In order to reduce electronic noise of the camera, six consecutive snapshots are averaged at the same location. The camera is translated on its trolley at several positions sequentially, in order to cover the whole length of the channel. This way, up to 20 pictures are captured along the channel, so that two consecutive pictures overlap by approximately 20%. This whole set of pictures is captured within less than 20 s, while the foam has moved by less than one cell diameter, thus offering an overall view of the foam in the channel at a given instant of time.

The scanning operation is repeated at a regular time interval (a time delay of about 100 s has been chosen) in order to follow the foam evolution. Data are recorded for a long period (up to 15 h representing the equivalent of 600 scans) in order to accumulate statistics. During that time period, the injection conditions were kept constant. The mandatory condition was checked *a posteriori* by measuring the drift velocity of the foam, and the cell area near the injection point, at several consecutive instants of the experiment. Runs presenting deviations smaller than 5% were considered as valuable, as those analysed here.

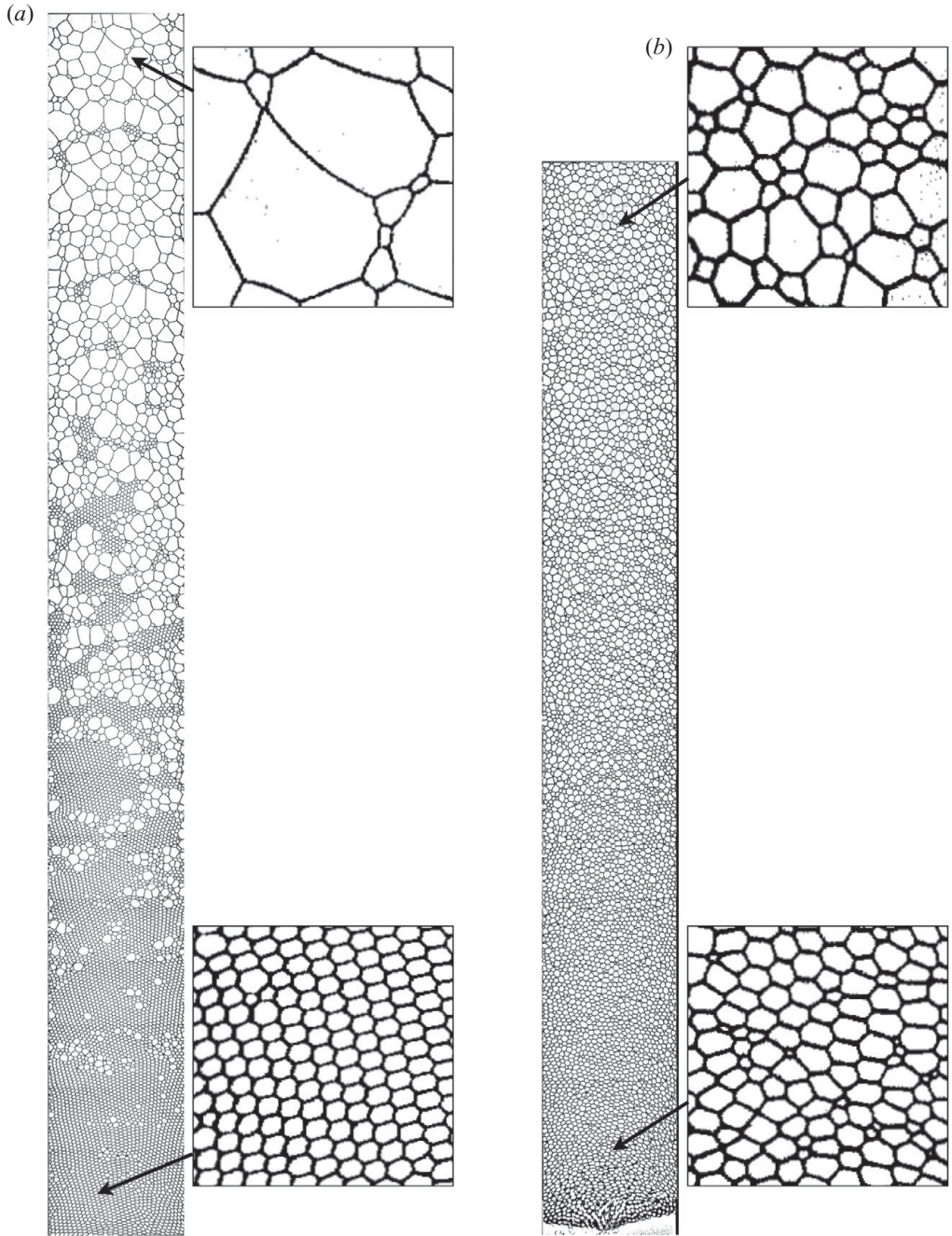


FIGURE 3. Instantaneous snapshots of foams in the channel. The image width is 20 cm, and its length is about 2 m. (a) Run *M*, initially monodispersed foam. Time runs from bottom ( $t=0$  min) to top ( $t=120$  min). (b) Run *P*, initially polydispersed foam (from  $t=0$  min to  $t=45$  min).

The channel is backlit by illuminating a white screen and the foam is imaged by transparency (figure 1). On an acquired image, foam cells appear clearly: the gas bubbles fill entirely the gap between the channel walls, only a thin film wets over the wall. A liquid separatrix separates two neighbour cells. This separatrix is found to be very thin ( $h \approx 40$  nm, see §4.1) and is not directly visible on the foam picture. The reason is that these liquid separatrices are connected to the channel walls by a meniscus of width ranging from 0.1 to 1 mm which, deviating light, appears dark and delimits the cells effectively.

The instantaneous foam picture is divided by a reference picture of the lighting background and the result is thresholded in order to obtain a binary picture of the foam structure. Finally, the local pictures set are stitched to each other to obtain a global reconstitution of the foam structure along the channel for a given instant of time in the form of a high resolution ( $6000 \times 640$ ) image (see figure 3), and then for all consecutive times.

### 2.3. Pre-processing

From the instantaneous binary picture of the foam structure obtained as explained above, the cells borders (the menisci) appear as lines up to 1 mm thick, and are not very regular: near the injection point, the foam is still very wet and the menisci are thick. As the foam ages, it also becomes dryer, and the menisci become thinner.

A watershed algorithm is used to obtain a skeleton of the foam structure. This image processing segmentation algorithm splits the image into connected areas corresponding to the foam cells. The latter are labelled, so that each cell is clearly identified on the instantaneous capture. Cell characteristics such as the centre of mass position, area  $S$ , perimeter length and number of facets  $n$ , are thus easily obtained. The major incertitude for determining these quantities is the exact position of the cell separatrix, which we assumed to be at the centre of the apparent meniscus. The error made on the position of the separatrix is estimated to be smaller than one pixel (corresponding to 0.3 mm), leading to a maximal error for the determination of the cell area of about 5%. The number of facets of a cell, which is equal to the number of neighbour cells (see figure 4), is, due to its discrete nature, accurately determined.

Since the high-resolution images of the foam have been acquired at different consecutive instants of time, the time series of foam evolution is also available. The tracking protocol of each individual cell from one instant to the other is divided into the following two steps.

(i) First, a PIV-like algorithm is used to determine the local average displacement of the foam ( $\delta X, \delta Y$ ). The centre of mass ( $X, Y$ ) of the cell is measured at time  $t$ . If the new position ( $X + \delta X, Y + \delta Y$ ) at time  $t + \delta t$  corresponds to the centre of mass of one cell within an error of one-tenth diameter, then the cell is identified. At this stage, almost half the cells are identified.

(ii) A second recursive step is performed for the remaining unidentified cells. Foam cells that have at least three common identified neighbours at time  $t$  and  $t + \delta t$  are assumed to be of the same cell. At the end of this recursive process, more than 98% of the cells are identified.

This protocol is illustrated for four consecutive image captures in figure 4. This tracking protocol was handily checked over 100 randomly chosen cells, tracked over eight time steps. Only one error was found, and this error concerned a ‘stock cell’ in the core of an island (to be defined in §3.3.1). In this case, the cells arrange themselves in a quasi-perfect lattice, where all the cells have the same area  $S$  and the same number of facets ( $n = 6$ ), so that the error has no consequence. The time

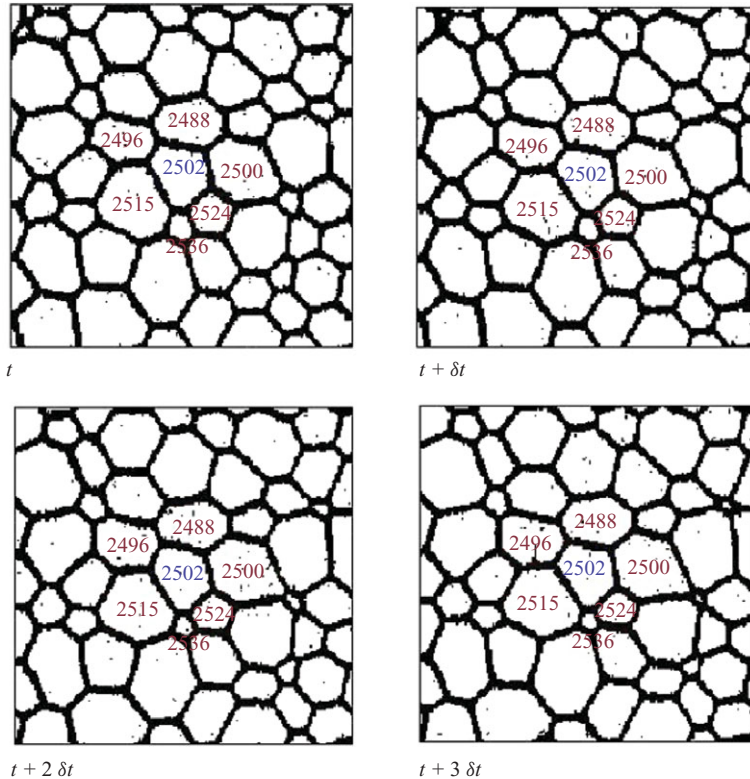


FIGURE 4. (Colour online) Tracking of foam cells for run *P*: cell no. 2502 is tracked over four consecutive snapshots. Its neighbour cells are also identified.

evolution characteristics of all the cells are stored in a database (available on demand) for their subsequent analysis.

#### 2.4. Experiments and parameters

We present experimental results obtained for two different runs that differ drastically regarding their initial conditions: in run *M*, the distribution of cell area at the injection is peaked, close to monodisperse, whereas the cell area is broadly distributed in run *P*. The experimental conditions are summarized in table 1.

### 3. Collective properties

#### 3.1. Area and facet number distributions

##### 3.1.1. Initially monodispersed foam

A foam is composed of a multitude of cells that are characterized in two dimensions, by their area  $S$  and their facet number  $n$ . In the case of a perfect lattice, all the cells have the same area, and have six facets. The initial state of run *M* is close to that simplistic limit. However, foam ageing results in a more complex state, where the area and facet number are more and more broadly distributed. Figure 5 illustrates this evolution. The initial area distribution is a Dirac delta around the area  $S_0$  of the injected cells,

$$P(S, t = 0) \approx \delta(S - S_0), \quad (3.1)$$



Experiment label	$M$	$P$
Type	Mono	Poly
Number of snapshots	600	300
Total number of cells	174 000	152 000
Initial area $\langle S_0 \rangle$	22 mm <sup>2</sup>	36 mm <sup>2</sup>
Velocity $U_T$	0.9 m h <sup>-1</sup>	2 m h <sup>-1</sup>
Travel time	120 min	45 min
Wall thickness	40 nm	60 nm
$\dot{S}^*$	140 mm h <sup>-2</sup>	95 mm h <sup>-2</sup>
$\alpha$	0–0.7/h	3/h–0.8/h
$\beta$	0.8/h	0.1/h
$\beta t_{max}$	1.6	Self-similar regime

TABLE 1. Summary of the experimental parameters.

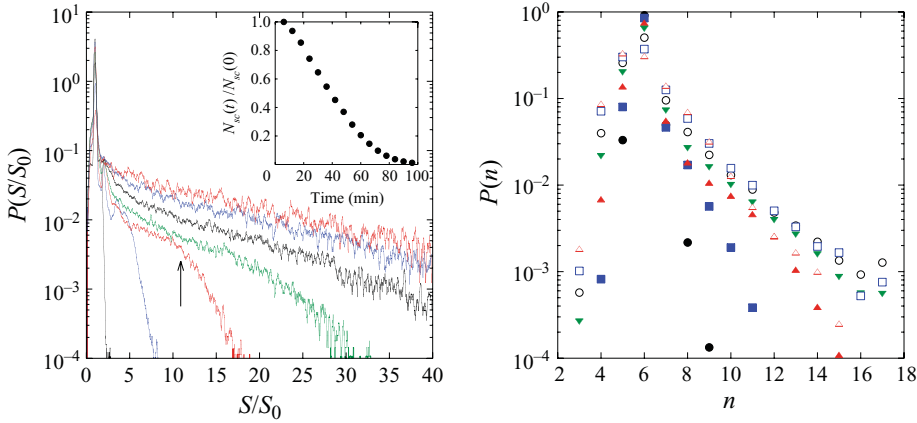


FIGURE 5. Cell area and facet number distributions in run  $M$  at several times ( $t = 6, 24, 42, 66, 78, 96, 114$  min).  $t = 6$  ( $\bullet$ ),  $24$  ( $\blacksquare$ ),  $42$  ( $\blacktriangle$ ),  $66$  ( $\blacktriangledown$ ),  $78$  ( $\circ$ ),  $96$  ( $\square$ ),  $114$  ( $\triangle$ ) min. The arrow indicates the value of  $S_{cutoff}/S_0$  at  $t = 42$  min. Inset: evolution of the relative stock cells reservoir population.

whereas the corresponding facet distribution is null except for  $n = 6$ , so that

$$P(n, t = 0) \approx \delta(n - 6). \quad (3.2)$$

At larger times  $t$ , the facet number distribution  $P(n, t)$  becomes broader, due to the morphological changes of the foam (see §4.2);  $P(n, t)$  has a maximum at  $n = 6$  at all times, and decreases exponentially, at larger  $n$ . The area distribution  $P(S, t)$  exhibits a large amount of cells with area  $S_0$  which also have six facets (the excess of 6-facet cells can be seen on  $P(n)$ , but due to the discrete nature of the facet distribution, this is less visible than on the area distribution). These cells have experienced no evolution from the initial state to the current time  $t$ , and their relative number  $N_{sc}(t)/N_{sc}(0)$  decreases at a fairly constant rate, as seen in figure 5. They are grouped into compact islands. The role of these ‘stock cells’ reservoir is discussed in §3.3.1. The area distributions  $P(S, t)$  present a nearly exponential decrease for intermediate areas, with a rapid fall-off at large  $S$ . It does not, however, exhibit any self-similar shape, since the characteristic area of the exponential decrease part of the distribution, and

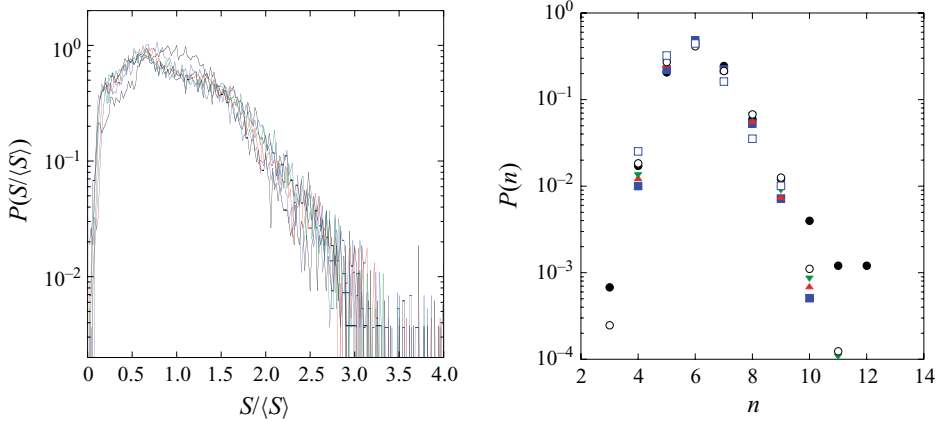


FIGURE 6. (Colour online) Cell area and facet number distribution in run  $P$  at several times  $t = 3$  ( $\bullet$ ), 11 ( $\blacksquare$ ), 20 ( $\blacktriangle$ ), 28 ( $\blacktriangledown$ ), 36 ( $\circ$ ), 45 ( $\square$ ) min.

that of the cutoff area are not proportional. For run  $M$ , the distribution  $P(S, t)$  is thus composed of three parts:

- (i) a Dirac delta at  $S = S_0$ ,
- (ii) a weak exponential decrease for  $S < S_{cutoff}$ ,
- (iii) a sharp decrease for  $S > S_{cutoff}$ .

In this case, the average area  $\langle S \rangle$  is not very meaningful: the total area of the foam being conserved through its evolution,  $\langle S \rangle$  is inversely proportional to the total number of cells, which includes the ‘stock cell’ reservoirs. It will be shown below that the dynamics of foam ageing occur outside of these reservoirs, so that we can exclude these cells from the statistics. Let  $\langle S_{rest} \rangle$  be the average area of the cells outside from the reservoirs. Since the exponential decrease of  $P(S, t)$  is mild for  $S < S_{cutoff}$ , one has  $\langle S_{rest} \rangle \approx S_{cutoff}$ . The measurement of  $S_{cutoff}$  thus provides a good measurement of the average foam evolution, and figure 7 shows that this characteristic area grows like  $t^{3/2}$ .

### 3.1.2. Initially polydispersed foam

Starting with a foam composed of cells with distributed area, as is the case for run  $P$ , the evolution shortcuts the transient stage of the ‘stock cells’ reservoir’s disappearance, which is an artifact of the monodispersed injection condition. Here, the foam is initially very disordered, with a rounded shape area distribution  $P(S, t=0)$  centred around its initial average. Roughly, one half of the cells have six facets (note that this category exceeds 92% for the monodispersed run  $M$ ), one quarter have five facets and the last quarter have seven facets. The average facet number is conserved during all the experiments ( $\langle n \rangle \approx 6$ , consistently with Euler’s theorem, see the pedagogical discussion in Bohn, Douady & Couder 2005). Figure 6 shows the facet number distribution to be nearly steady, and presents a slight dissymmetry favouring the facet numbers  $n > 6$ .

The area  $P(S, t)$  distributions are shown in figure 6 versus  $S$  rescaled by the current average area  $\langle S \rangle$ , which grows linearly with time ( $d\langle S \rangle/dt \approx 85 \text{ mm}^2 \text{ h}^{-1}$ ). In these coordinates, it appears that the area distribution tends towards a self-similar shape: the initial round-shaped distribution flattens for  $0.5 < S/\langle S \rangle < 1.5$  at larger time. For

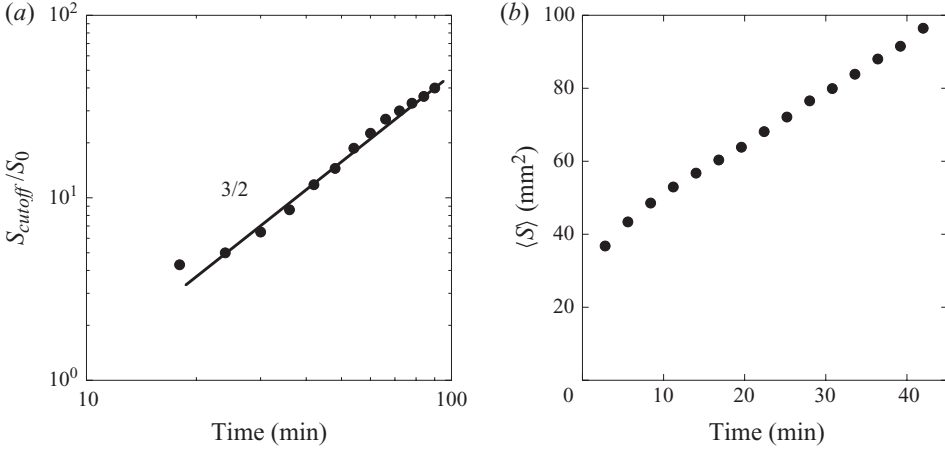


FIGURE 7. (a) Cutoff area in run *M* (initially quasi-monodispersed foam with  $S_0 = 22 \text{ mm}^2$ ) and (b) average area for run *P*, initially polydispersed case.

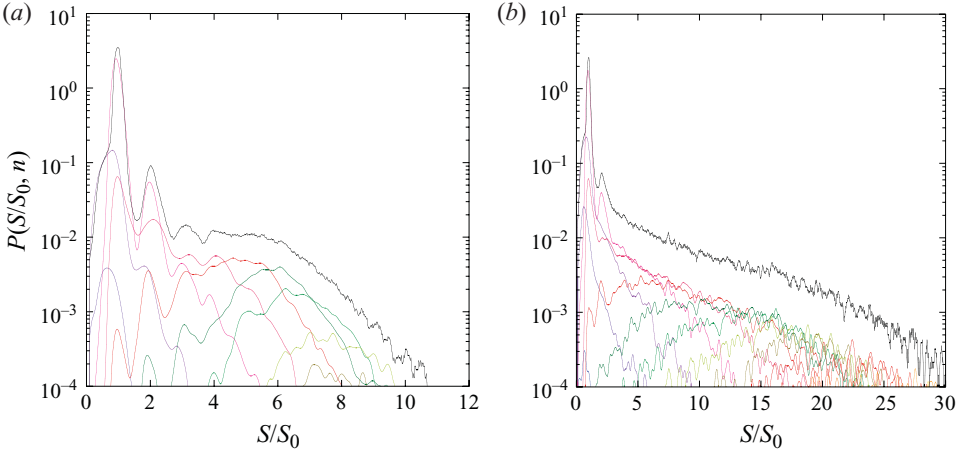


FIGURE 8. (Colour online) Distributions  $P(S, n)$  at time  $t = 30 \text{ min}$  ((a),  $n$  is varied from 3 to 12) and  $t = 60 \text{ min}$  ((b),  $n$  is varied from 3 to 17), for run *M*.

$S/\langle S \rangle > 1.5$ , the probability  $P(S/\langle S \rangle)$  decreases rapidly. Consequently, the distribution area cutoff scales like  $\langle S \rangle$ , a signature of self-similarity (figure 7).

### 3.2. Conditional expectation, Lewis law

As can be seen in figure 3, large cells have a large number of facets. Quantitatively, figure 8 shows  $P(S, n)$ , the repartition of the cell area distribution with the number  $n$  of facets.  $P(S, n)$  is the probability density that a cell has an area between  $S$  and  $S+dS$ , and a number of facets equal to  $n$ . It is related to the conditional probability by

$$P(S, n) = P(n)P(S|n). \quad (3.3)$$

The distribution  $P(S, n)$  is then normalized with respect to an integration over  $S$  and a summation over  $n$ . By definition, one also has

$$P(S) = \sum_{n=0}^{+\infty} P(S, n). \quad (3.4)$$

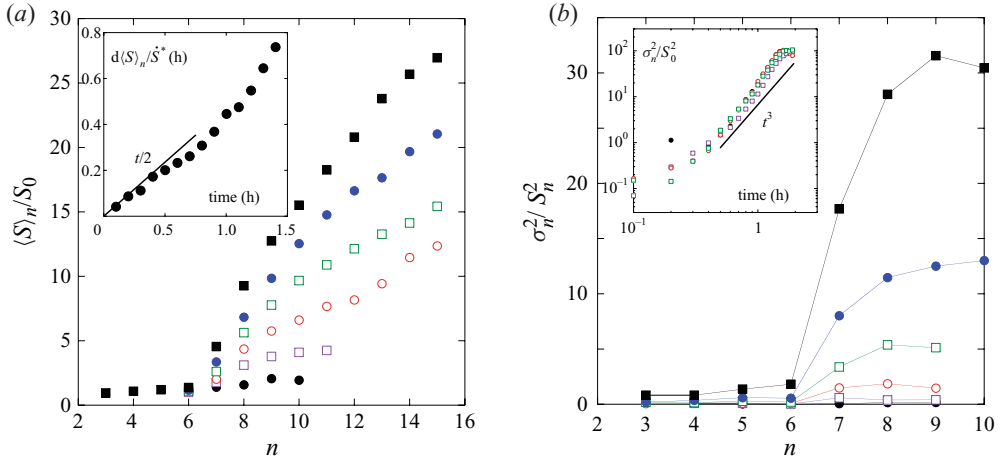


FIGURE 9. (Colour online) Average area  $\langle S \rangle_n$  (a) and variance  $\sigma_n^2$  (b) at times  $t = 6$  (●), 18 (□), 30 (○), 42 (◻), 54 (●), 66 (■) min, for run **M**. Inset: the time evolution of these quantities.

For small facet numbers ( $n \leq 6$ ),  $P(S, n)$  is a decreasing function of  $S$ , close to an exponential. For larger  $n$ ,  $P(S, n)$  is rounder, with a most probable value increasing with  $n$ . One may define the conditional average and variance (figure 9)

$$\langle S \rangle_n = \int S P(S|n) dS, \quad (3.5a)$$

$$\sigma_n^2 = \int S^2 P(S|n) dS - \langle S \rangle_n^2. \quad (3.5b)$$

Note that for  $n = 6$ , these quantities are affected by the ‘stock cells reservoirs’ (in run **M**). Figure 9 shows that  $\langle S \rangle_n$  grows linearly with  $n$  for  $n \geq 6$ . This is known as Lewis law (Lewis 1928).

The dependence of  $\langle S \rangle_n$  on  $n$ , measured by the derivative  $d\langle S \rangle_n / dn$  is found to be a linearly increasing function of time. The variance  $\sigma_n^2$  appears to be nearly independent of  $n$ , for  $n > 6$ , and an increasing function of time. For  $n = 6$ ,  $\sigma_n^2$  is artificially small, due to large amount of ‘stock cells’. For run **M**, one has

$$\langle S \rangle_n \approx (n - 3) \dot{S}^* t / 2, \quad (3.6a)$$

where  $\dot{S}^*$  is the von Neumann’s area increase velocity (see §4.1) and

$$\sigma_n^2 \propto t^3. \quad (3.6b)$$

In run **P**,  $\langle S \rangle_n$  and  $\sigma_n^2$  are linear functions of  $n$  (figure 10). These quantities scale in time like  $\langle S \rangle$  so that

$$\langle S \rangle_n \approx 0.35(n - 3) \langle S \rangle \quad (3.7a)$$

and

$$\sigma_n^2 \approx 0.04(n - 3) \langle S \rangle^2. \quad (3.7b)$$

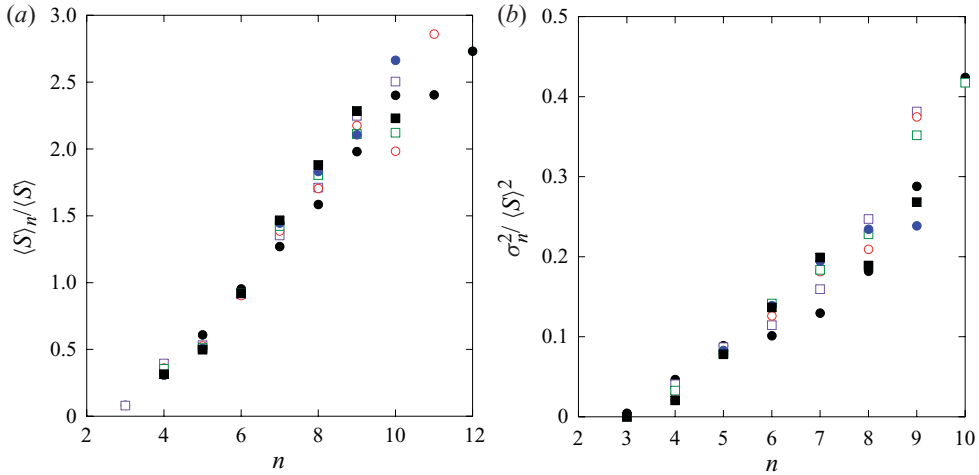


FIGURE 10. (Colour online) Average area  $\langle S \rangle_n$  (a) and variance  $\sigma_n^2$  (b) at times  $t=3$  (●), 10 (□), 15 (○), 20 (□), 25 (●), 30 (■) min, for run *P*. Each quantity scale on the average area  $\langle S \rangle$ , which itself scales like time  $t$ .

### 3.3. Environment properties

#### 3.3.1. Stock cells reservoirs

The foam can be viewed as a cluster of individual cells. When the cells are initially monodispersed, this cluster is a (nearly) perfect crystal. Local defects generate reorganizations of the cells arrangement through  $\mathcal{T}_1$  and  $\mathcal{T}_2$  processes (see §4.2). These topological modifications are the first step of the foam ageing, which thus results from localized processes. Consequently, the foam regions with no default do not age (see also the discussion by Glazier *et al.* 1987), and persist as subregions of cells arranged in a perfect lattice; These sub-clusters are the ‘stock cells reservoir’.

The true ageing dynamic of the foam occurs outside of these reservoirs, where some cells grow, while other vanish, in a disordered fashion. At the border of the reservoir, the ‘stock cells’ are exposed to this disorder, and may suffer  $\mathcal{T}_1$  process (see §4.2). Such cells are thus likely to be included in the aged part of the foam. The reservoirs are thus progressively eroded, and figure 3 shows that the reservoir represents the largest part of the foam in the earliest stage (more than 92%), and that it progressively reduces to unconnected clusters which have, however, not completely disappeared at the latest stages we have investigated.

The population of stock cells  $N_{sc}(t)$  decreases with time nearly exponentially, as shown in figure 5, until the reservoir empties. The number of stock cells injected in the ageing part of the foam per unit time is thus decreasing in time.

#### 3.3.2. The aged foam: a disordered medium

Since all stock cells are found in reservoirs, these are most probably surrounded by other stock cells. The crystal-like environment of stock cells is thus very correlated. On the contrary, the aged foam composed of the cells outside the reservoir appears very unordered. Figure 11 shows the area distribution  $P_n(S)$  of the first neighbours of cells with a fixed facet number  $n$ . At the notable exception of  $n=6$  facet cells, which include the stocks cells reservoir, these distributions essentially collapse. The  $n=6$  facets cells are split into two categories: the stock cells and the others. Excluding stock cells of the statistics (i.e. excluding cells with area  $S_0$ ) would lead to a global

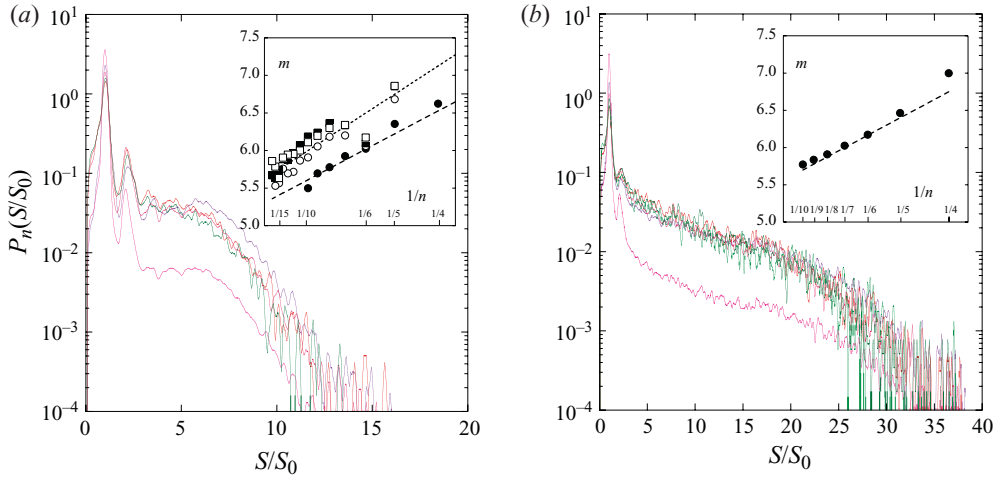


FIGURE 11. (Colour online)  $P_n(S)$  at time  $t = 30$  min (a) and  $t = 60$  min (b) of run  $\mathbf{M}$ .  $n$  is varied from 5 to 9. At the notable exception of  $n = 6$ , all the curve collapses. The stock cell (with area  $S_0$ ) is overrepresented in the neighbourhood of six facets cells (that are essentially other stock cells.) Insets: evolution of  $m$ , the neighbours' mean facet number and comparison with Aboav law. (a) Run  $\mathbf{M}$ ,  $m(n)$  is plotted for time  $t = 12, 36, 60, 84$  min, and the Aboav–Weaire law is plotted for time  $t = 12$  min ( $\mathcal{A} = 1, \mu_2 \approx 0.1$ ) and time  $t = 84$  min ( $\mathcal{A} = 0.75, \mu_2 \approx 3.0$ ). (b) Run  $\mathbf{P}$ :  $m(n)$  is an independent function of time, and a mean result is presented.  $\mathcal{A} = 1, \mu_2 \approx 0.9$ .

collapse of all  $P_n$ . These observations suggest that a single cell in the foam basically evolves in a surrounding medium whose properties are that of the mean. Adjacent cells at a given instant of time ('survivors') have indeed been observed to be initially distant from each other, separated by many other cells which have in the meantime disappeared (Levitan *et al.* 1994), also suggesting that adjacent cells have had a basically uncorrelated history.

### 3.3.3. The Aboav-Weaire law

However, the foam is not a totally uncorrelated medium. Aboav (1980) has observed that the average facet number  $m(n)$  of the neighbours cells depends on its number of facet  $n$ . The number  $m(n)$  is a decreasing function of  $n$ , as a consequence of geometrical constraints. A correlation of the form

$$m(n) = A + \frac{B}{n}, \quad (3.8)$$

where  $A$  and  $B$  are constants, is usually observed. Weaire & Hutzler (1999) show that, assuming the shape of  $m(n)$ , impose that  $A$  and  $B$  are fixed. In a simple form, it is found that

$$m(n) = 6 - \mathcal{A} + \frac{6\mathcal{A} + \mu_2}{n}, \quad (3.9)$$

where  $\mathcal{A}$  is a free parameter and  $\mu_2$  is the second moment of the facet number distribution  $P(n)$ . Our experimental data are compatible with these correlations, although the agreement is not perfect. In the case of run  $\mathbf{M}$ , the free parameter  $\mathcal{A}$  is found to be of order 0.75, which is an unusually small value for soap froth (Weaire & Hutzler 1999 report a value closer to 1.2). The coexistence of well-ordered island (the stock cells reservoir) with disordered foam may be at the origin of this unusual value.

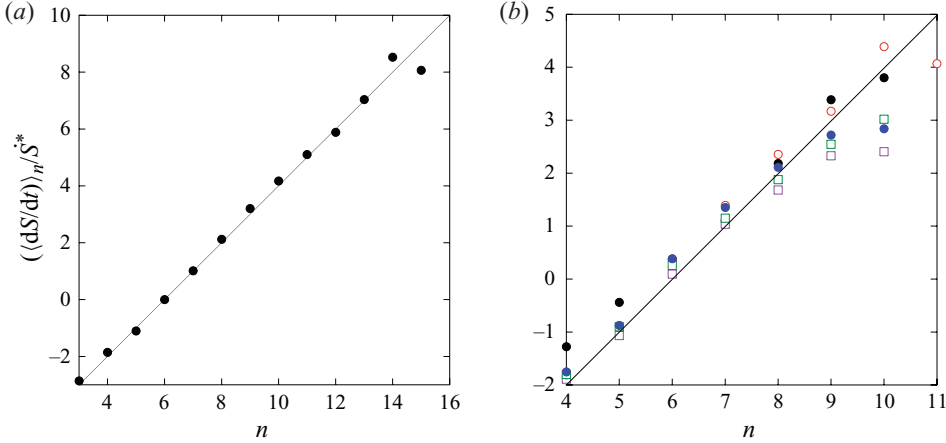


FIGURE 12. (Colour online) Individual cell area variation. (a) Run **M**, individual  $dS_n/dt$  are averaged over the whole experiment (all time),  $\dot{S}^*$  is measured at  $140 \text{ mm}^2 \text{ h}^{-1}$ . (b) Run **P**, individual  $dS_n/dt$  are averaged for fixed times  $t = 5$  (●),  $15$  (□),  $25$  (○),  $35$  (□), and  $45$  (●) min,  $\dot{S}^* = 95 \text{ mm}^2 \text{ h}^{-1}$ .

Nevertheless,  $m(n)$  lies between  $6 - \mathcal{A}$  for large  $n$ , and  $6 + \mathcal{A} + \mu_2/3$  for  $n = 3$ . The largest portion of the cell population has a number of facets  $n$  included between 5 and 7 (see, e.g. run **P**), corresponding to a difference in  $m(n)$  of roughly 0.4. This variation in the neighbourhood features is weaker than the global fluctuation in the whole medium ( $\mu_2 = 0.9$ ). This is consistent with the observations of §3.3.2, and supports a ‘mean field’ description of the interactions between cells in the foam.

#### 4. Individual cell evolution properties

The local evolution of the foam is governed by two kinds of elementary processes: mass exchange of gas between neighbour cells is responsible for their growth and decay in area, while topological changes known as  $\mathcal{T}_1$  and  $\mathcal{T}_2$  processes induce changes in facet number.

##### 4.1. von Neumann’s law

The area variation of a cell in a two-dimensional foam was first described by von Neumann (1952). The pressure difference between neighbour cells leads to a chemical unbalance through the cell walls: the concentration of dissolved gas is proportional to the vapour pressure inside the cell, so that a concentration gradient appears inside the wall, and thus a mass flux by Fick diffusion. The area variation of a cell is proportional to the net mass flux exchanged with all its neighbours. von Neumann showed that this net mass flux is given by its number  $n$  of facets so that

$$\frac{dS}{dt} = \dot{S}^* (n - 6), \quad (4.1)$$

where  $\dot{S}^*$  depends on the foam characteristics (see details in Appendix A) and is measured from figure 12.

##### 4.2. Topological changes

###### 4.2.1. $\mathcal{T}_2$ process

Foam cells having less than six facets decrease in area. This process ends by the cell disappearance. Most commonly, at the last stages, the foam has reorganized so that

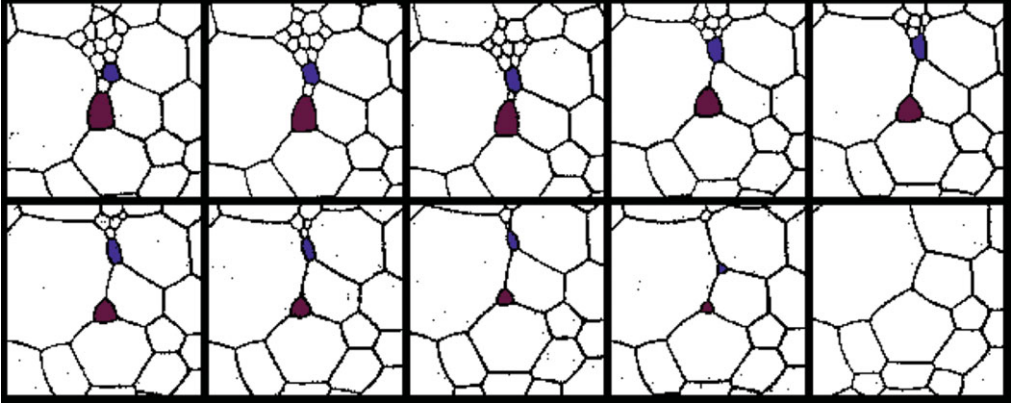


FIGURE 13. (Colour online)  $\mathcal{T}_2$  process in run  $M$ . Snapshots are separated by 106 s.

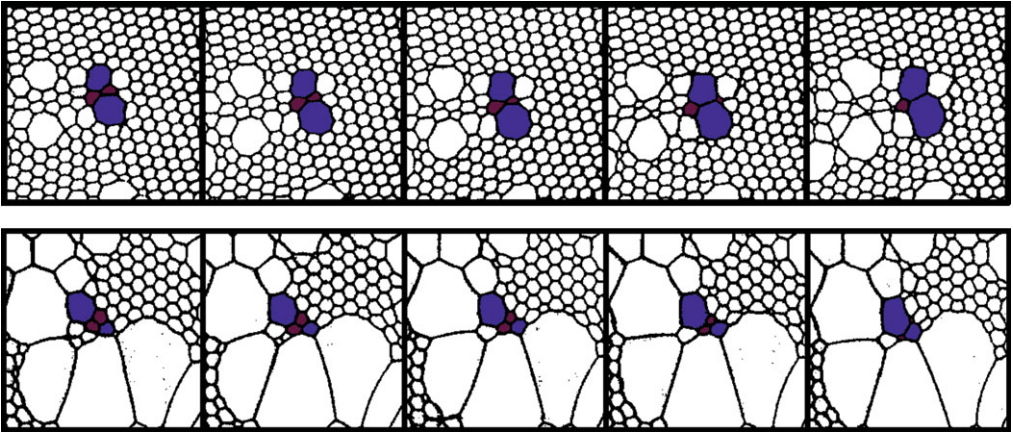


FIGURE 14. (Colour online) Several  $\mathcal{T}_1$  processes (run  $M$ ). Snapshots are separated by 106 s.

the cells vanish having three facets (see §4.2.2). Rarely two facet cells are observed. An example of  $\mathcal{T}_2$  process is given in figure 13. The consequences of the  $\mathcal{T}_2$  process is, besides the disappearance of one cell, that its last three neighbours all lose 1 facet. The total number of facets in the foam is then reduced by six (three neighbours lose one facet, and the disappearing cell loses three facets) when the total number of cells is reduced by 1. Consequently, the average number of facets  $\langle n \rangle$  is conserved if it is equal to 6. This equilibrium is unstable since

$$\left. \begin{aligned} \langle n \rangle = 6 &\implies \delta \langle n \rangle = 0, \\ \langle n \rangle < 6 &\implies \delta \langle n \rangle < 0, \\ \langle n \rangle > 6 &\implies \delta \langle n \rangle > 0, \end{aligned} \right\} \quad (4.2)$$

these relations holding for the whole set of cells. For the surviving cells, one has of course  $\langle \delta n \rangle = -1$ .

#### 4.2.2. $\mathcal{T}_1$ process

Another topological process, named  $\mathcal{T}_1$ , occurs in the foam. This process concerns four cells that swap their neighbourhood (see figure 14: initially, cells A and B are neighbours, while C and D are common neighbours of A and B. After the  $\mathcal{T}_1$  process,



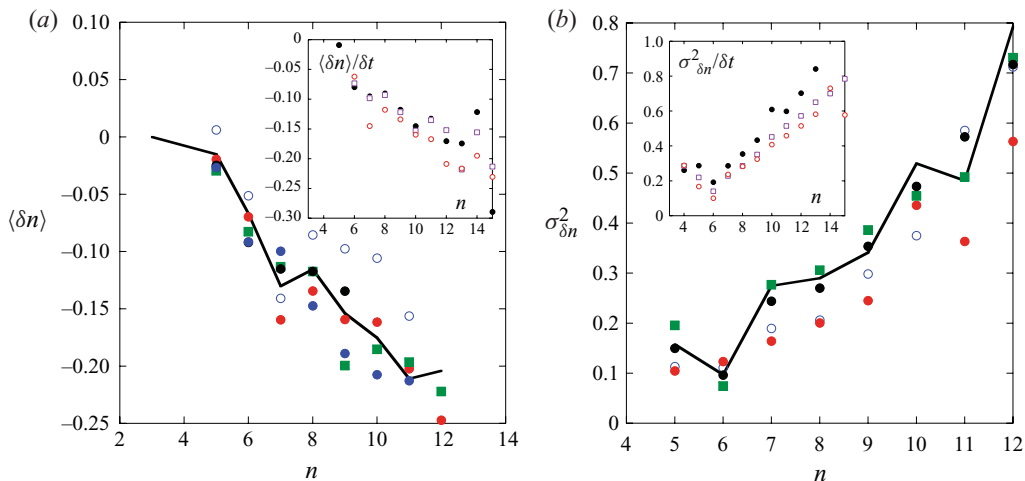


FIGURE 15. (Colour online) (a) Average and (b) variance of  $\delta n$ , the variation of the number of facets of cells with initially  $n$  facets.  $\delta n$  is estimated on two consecutive snapshots (separated by 106 s). The continuous line represents the average statistics for time  $1 \text{ h} \leq t \leq 2 \text{ h}$ , dots,  $t = 60$  (○), 80 (●), 100 (■), 110 (●), 120 (●) min. Insets: average and variance of  $\delta n$ , the variation of the number of facets of cells with initially  $n$  facets, over a time  $\delta t$ . ( $\delta t$  is varied from one to three consecutive snapshots (106 s ●, 212 □, 318 ○s)). The data are taken for time  $1 \text{ h} \leq t \leq 2 \text{ h}$  in run *M*.

A and B are no more neighbours, even if they remain common neighbours of C and D. Cells C and D have become neighbours. In such a process, A, B lose one facet while C, D gain one facet. The  $\mathcal{T}_1$  process is thus an exchange of one facet between cells

$$\left. \begin{aligned} n'_{A,B} &= n_{A,B} - 1, \\ n'_{C,D} &= n_{C,D} + 1. \end{aligned} \right\} \quad (4.3)$$

The average number of the facet distribution is conserved

$$\langle \delta n \rangle = 0 \quad (4.4)$$

but its variance has increased

$$\sigma_{\delta n}^2 = 1. \quad (4.5)$$

Note that the characteristic time of such a process has been found in dry foams to be of the order of seconds (Durand & Stone 2006), a time interval much shorter than the one of the global coarsening process (lasting hours).

#### 4.2.3. Consequences on the facet number distribution

The major consequence of these topological processes is that the facet number distribution is modified. The observed variation  $\delta n$  for a given cell between two snapshots lies most probably in the set  $\{-1, 0, +1\}$ . Figure 15 shows the average value and the variance of  $\delta n$  for a fixed initial cell facet number. A linear dependence on  $n$  is found

$$\langle \delta n \rangle_n \approx -a(t)[n - 3], \quad (4.6a)$$

$$\sigma_{\delta n}^2 \approx b(t)[n - 3]. \quad (4.6b)$$

The origin of the facet number variation lies in the  $\mathcal{T}_1$  and  $\mathcal{T}_2$  processes. The first one is at the origin of the broadening of the distribution of  $n$ , without changing the

mean  $\langle n \rangle$ , while the latter has for main effect to diminish  $\langle n \rangle$ . We have never observed spontaneous film breakage. We have shown (§3.3.2) that the local environment of one cell is statistically independent of the cell number of facets. A naive estimation of the probability of occurrence of topological processes in the direct neighbourhood of one cell is that it is proportional to its number of facets  $n$ . A small correction to this simple picture is however observed and the probability that a topological process occurs in the direct neighbourhood of one cell is rather proportional to  $n - 3$ . This fact might be a consequence of a spatial correlation, reported through Aboav's relationship (§3.3.3): small cells are, on average, surrounded by cells with an average facet number  $m(n)$  exceeding 6. In the neighbourhood of small cells,  $\mathcal{T}_2$  processes are thus unlikely. A longer correlation range may exist (Szeto, Aste & Tam 1998), and its consequence is embedded in (4.6). To summarize, this condition prevents topological modification of three-facet cells, and the number of facets of one cell cannot become smaller than 3.

Let  $\alpha[n - 3]$  and  $\beta[n - 3]$  be, respectively the rate of occurrence  $\mathcal{T}_2$  and  $\mathcal{T}_1$  processes, for a given cell. For a time interval  $\delta t$ , the distribution of  $\delta n$  is then of the form

$$P(\delta n, \delta t) = ((\alpha + \beta)[n - 3]\delta t\delta_{-1} + (1 - (\alpha + 2\beta)[n - 3]\delta t)\delta_0 + \beta[n - 3]\delta t\delta_{+1}), \quad (4.7)$$

and the effect on the averaged quantities is thus expected to be

$$\langle \delta n \rangle = -\alpha[n - 3]\delta t, \quad (4.8a)$$

$$\sigma_{\delta n}^2 = (\alpha + 2\beta)[n - 3]\delta t. \quad (4.8b)$$

Consequently,  $\alpha$  and  $\beta$  are deduced from  $a$  and  $b$  in (4.6) by

$$\left. \begin{aligned} \alpha &= a, \\ \beta &= (b - a)/2. \end{aligned} \right\} \quad (4.9)$$

At the first instant of run **M**, the estimation of  $a$  and  $b$  is difficult, since the number of cells with a number of facet higher than eight is small (so that the variation of  $\delta n$  with  $n$  is hardly measured). It seems that  $b$  is constant in time, as  $a$  grows from a very low value to its asymptotic value. For run **P**,  $b$  is close to  $a$  so that the estimation of  $\beta$  is not possible (figure 16).

## 5. Computing the cell surface distribution

Having determined the processes which affect cell size distribution, and measured their rates  $\alpha$  and  $\beta$ , we derive a mean field theory to compute the shape and evolution of  $P(S, n, t)$ .

### 5.1. A continuous model

The area and number of facet evolves through the process that we have just quantified. It is then possible to write the Fokker–Planck equation for the evolution of  $P(S, n, t)$

$$\begin{aligned} \partial_t P = \lim_{\delta t \rightarrow 0} \left[ -\partial_S \left( \left\langle \frac{\delta S}{\delta t} \middle| S, n \right\rangle P \right) - \partial_n \left( \left\langle \frac{\delta n}{\delta t} \middle| S, n \right\rangle P \right) \right. \\ \left. + \partial_n^2 \left( \left\langle \frac{\sigma_{\delta n}^2}{\delta t} \middle| S, n \right\rangle P \right) + \delta(S) \left\langle \frac{dS}{dt} \middle| S \right\rangle P \right], \quad (5.1) \end{aligned}$$

where the last term ensures that when a cell reaches an area  $S=0$  it disappears from the distribution. Consequently, the norm of  $P$  is not conserved, and  $P(S, t)$  should be

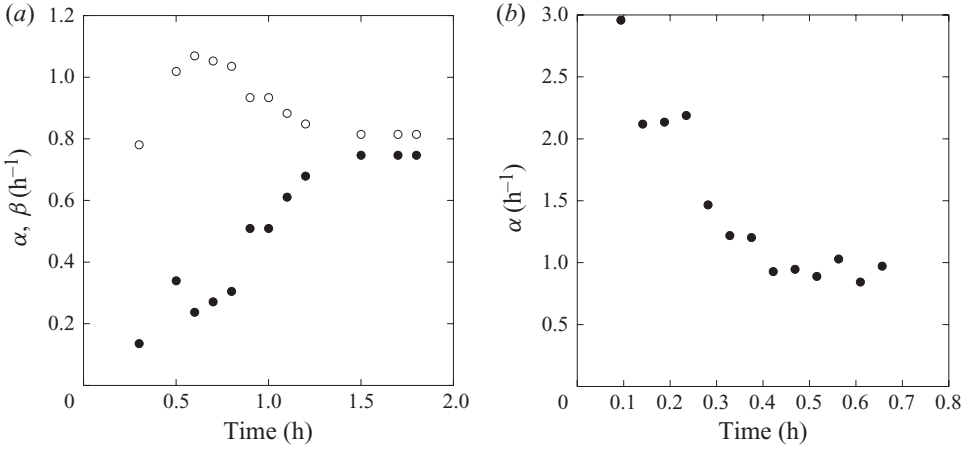


FIGURE 16. Computed values of  $\alpha$  (●) and  $\beta$  (○). (a) Run *M*, (b) Run *P*.  $\beta$  is found to be smaller than  $0.2 \text{ h}^{-1}$ , with no accuracy.

normalized by  $(\int dS \int dn P(S, n))^{-1}$  at each instant of time. However, this term leads to technical complications and is neglected in the following. The modelled distribution thus includes negative area cells that have no physical meaning. We just consider the distribution  $P(S, t)$  for  $S \geq 0$ . An error nevertheless remains: cells that have had a negative area for some time and which have recovered a positive area subsequently should not be considered. This flaw also affects Flyvbjerg (1993) formulation, which accounts for the normalization, but not for the presence of negative area cells. This leads to an overestimation of the probability distribution in the neighbourhood of  $S \approx 0$  for  $dS/dt > 0$  (cells with  $n > 6$ ). Fortunately, this probability is found to be very small, so that the error made is negligible.

### 5.2. The discrete problem

In (5.1),  $n$  is considered as a continuous variable. This approximation is crude near  $n = 3$ , since the first- and second-order moments of  $\delta n$  are proportional to  $n - 3$ . We thus consider the, fundamentally equivalent, but technically more precise following discrete version of the Fokker–Planck equation:

$$\begin{aligned} \partial_{\mathfrak{t}} P = & -(n - 6)\partial_{\mathfrak{S}} P + \check{\alpha} (([n - 3] + 1)P(\mathfrak{S}, n + 1, \mathfrak{t}) - [n - 3]P(\mathfrak{S}, n, \mathfrak{t})) \\ & + \check{\beta} (([n - 3] + 1)P(\mathfrak{S}, n + 1, \mathfrak{t}) + ([n - 3] - 1)P(\mathfrak{S}, n - 1, \mathfrak{t}) \\ & - 2[n - 3]P(\mathfrak{S}, n, \mathfrak{t})), \end{aligned} \quad (5.2)$$

with time and area made non-dimensional so that  $\check{\beta} = \beta/\beta$  equals unity and  $d\mathfrak{S}/d\mathfrak{t} = (n - 6)$ , i.e replacing time by  $\mathfrak{t} = \beta t$ . The dimensionless variables are thus

$$\left. \begin{aligned} \mathfrak{t} &= \beta t, \\ \mathfrak{S} &= \beta S / \dot{S}^*, \\ \check{\alpha} &= \alpha / \beta, \\ \check{\beta} &= 1. \end{aligned} \right\} \quad (5.3)$$

We address the asymptotic coarsening regime (of run *M* for instance, see figure 16), and we assume, for simplicity, that  $\alpha$  and  $\beta$  are constant in time. Let us consider the initial condition (cells having all  $n = 6$  with a given initial area distribution  $P_0(\mathfrak{S})$ )

$$P(\mathfrak{S}, n, \mathfrak{t} = 0) = P_0(\mathfrak{S})\delta(n - 6), \quad (5.4)$$

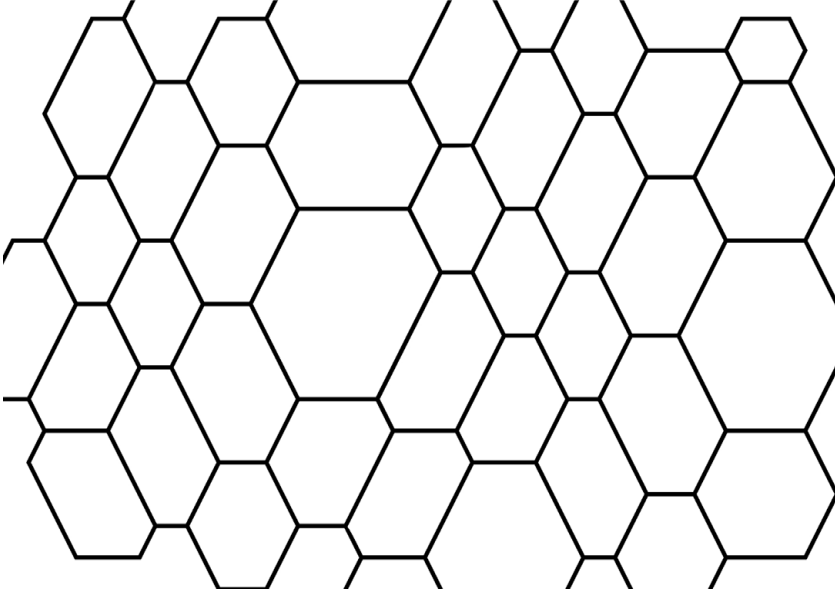


FIGURE 17. Foam composed of six-facet cells, with distributed area corresponding to the initial condition in (5.4).

which might correspond either to a perfect hexagonal lattice for a narrow surface distribution  $P_0(S)$ , or to a disordered medium with a broad surface distribution, as pictured in figure 17. The corresponding solution to (5.2) is (see Appendix B)

$$P(S, n, \mathbb{t}) = P_0(S) \otimes \delta(S + 3\mathbb{t}) \otimes \mathcal{Q}_-^{\otimes -3} \otimes \left( \sum_{i=0}^3 C_3^i C_{n+i-4}^2 \left( -\frac{\check{\alpha} + \check{\beta}}{\check{\beta}} \right)^i (\mathcal{Q}_- \otimes \mathcal{Q}_+)^{\otimes i} \right) \otimes \mathcal{Q}_+^{\otimes (n-3)}, \quad (5.5)$$

where  $\otimes$  denotes the convolution operator along  $S$ , and  $\mathcal{Q}_\pm$ , are functions of  $S$  given by their Fourier transform,

$$\bar{\mathcal{Q}}_\pm = \frac{2\check{\beta}}{\pm(\check{\alpha} + 2\check{\beta} + ik) + \frac{x}{\tan(x\mathbb{t}/2)}}, \quad (5.6)$$

with

$$x = \sqrt{-\check{\alpha}^2 - 2i\check{\alpha}k - 4i\check{\beta}k + k^2} = \sqrt{4\check{\beta}(\check{\alpha} + \check{\beta}) - (\check{\alpha} + 2\check{\beta} + ik)^2}. \quad (5.7)$$

The transfer function leading to  $P(S, n, \mathbb{t})$  decomposes in a summation of a Dirac delta function of decaying amplitude  $\exp(-(3\check{\alpha} + 6\check{\beta})\mathbb{t})\delta_{n,6}\delta(S)$ , and of a continuous distribution over  $S$ . The former term shows that cells with  $n=6$ , as the stock cells found in the ‘reservoirs’, do persist, even in a disordered foam.

### 5.3. Comparison with experimental data (run $M$ )

Equation (5.5) describes the evolution in time of the distribution  $P(S, n, t)$  of cell areas and facet number, for the initial condition given by (5.4). Run  $M$  is well described by this initial condition, except that stock cells are continuously injected in the ageing foam through the erosion of the reservoirs, as described in §3.3.1 and this

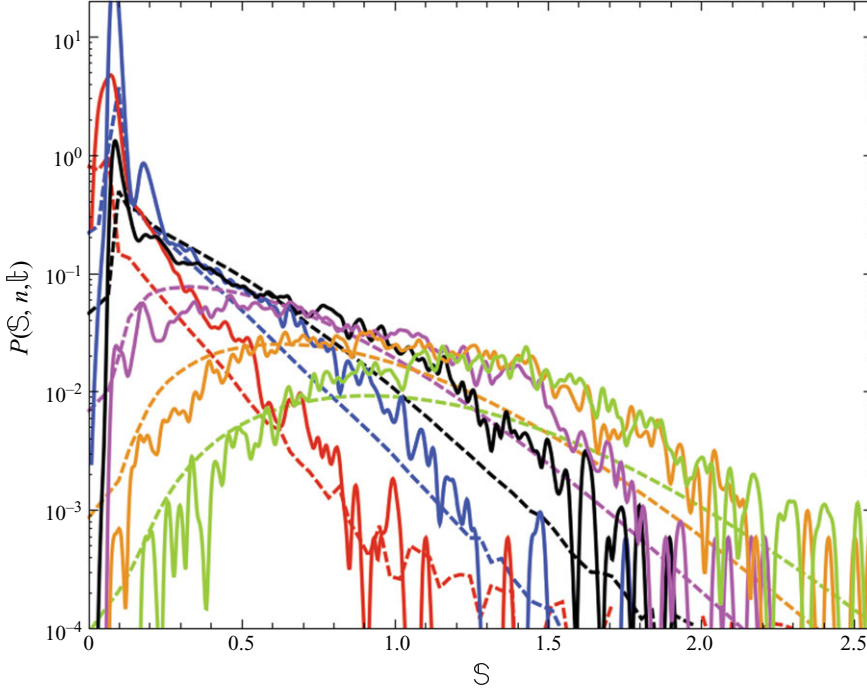


FIGURE 18. (Colour online)  $P(S, n, t)$  for run  $M$  at time  $t = 1$  h and comparison with the prediction in (5.10), for  $5 \leq n \leq 10$ .

over a long time, concomitantly with the ageing process of the rest of the foam which (5.5) intends to represent. Let  $I(t)$  be the injection rate of the stock cells. Since the evolution equation (5.2) is linear, the superposition principle applies, and the global cell area distribution  $P(S, n, t)$  is given by

$$P(S, n, t) = \int d\mathfrak{t} P(S, n, t - \mathfrak{t}) I(\mathfrak{t}), \quad (5.8)$$

where  $P(S, n, t)$  is given by the Green function in (5.5). Figure 5 shows the evolution of the amount  $N_{sc}(t)$  of remaining stock cells. The injection rate  $I(t)$  is thus

$$I(\mathfrak{t}) = -\frac{dN_{sc}(\mathfrak{t})}{d\mathfrak{t}}. \quad (5.9)$$

During the first 60 min of run  $M$ , the decrease of  $N_{sc}(t)$  is close to exponential, indicating a decreasing rate of stock cell injection  $I(t)$ . In the time interval corresponding to stock cell injection,  $\alpha$  is a linearly increasing function of time, as seen in figure 16; it reaches a constant after  $t = 1$  h. The experimental data are thus compared with

$$\sum_{i=0}^9 \mathcal{I}^i P\left(S, n, t \frac{9.5 - i}{10}\right) \Big|_{(\tilde{\alpha} \frac{i+1}{10}, \beta)}, \quad (5.10)$$

with  $\mathcal{I} = 0.9$  being the injection rate of stock cells,  $\alpha = 0.65 \text{ h}^{-1}$  and  $\beta = 0.8 \text{ h}^{-1}$ , data that are compatible with the experimental values in figure 16.

The computation of  $P(S, n, t)$  is made through a numerical evaluation of the Fourier transform of  $\bar{P}(k, n, t)$ . As seen in figure 18, the agreement is not perfect, but

a qualitative agreement is reached, suggesting that the main physical aspects of the problem have been captured.

#### 5.4. Distribution of the number of facets $P(n)$

The distribution  $P(S, n, \mathbb{t})$  given in (5.5) includes negative area cells ( $S < 0$ ). The distribution  $P(n, t)$  of the number of facets can be deduced from the global distribution and, up to a normalization factor, one has

$$P(n, t) \propto \int_0^{+\infty} dS P(S, n, \mathbb{t}). \quad (5.11)$$

However, as can be seen from the comparison in § 5.3 and figure 18, the predicted distribution  $P(S, n, \mathbb{t})$  has non-negligible probability for negative area cells only for cells with a small number of facets ( $n \leq 6$ ), so that for larger  $n$ , the following approximation holds:

$$P(n, \mathbb{t}) \approx \int_{-\infty}^{+\infty} dS P(S, n, \mathbb{t}), \quad (5.12)$$

which turns out to be the zero-mode of the Fourier Transform  $\bar{P}(k=0, n, \mathbb{t})$ ,

$$P(n, \mathbb{t}) \approx \frac{4\check{\beta}^2}{\left(\frac{\check{\alpha}^2}{\tan h(\check{\alpha}\mathbb{t}/2)}\right)^2 - (\check{\alpha} + 2\check{\beta})^2} \left( \sum_{i=0}^3 C_3^i C_{n+i-4}^2 \left( -\frac{\check{\alpha} + \check{\beta}}{\check{\beta}} \right)^i \right) \times \left[ \frac{2\check{\beta}}{(\check{\alpha} + 2\check{\beta}) + \frac{\check{\alpha}}{\tan h(\check{\alpha}\mathbb{t}/2)}} \right]^{n-6} \quad (5.13)$$

holding for  $n \geq 7$ . This is the sum of Gamma distributions of orders 0, 1, 2 and 3, which presents an exponential tail at large  $n$ ,

$$P(n, \mathbb{t}) \propto \left( \frac{2\check{\beta}}{(\check{\alpha} + 2\check{\beta}) + \check{\alpha}/\tan h(\check{\alpha}\mathbb{t}/2)} \right)^n, \quad (5.14)$$

consistently with the observed shape of  $P(n, t)$ , as seen from figures 5 and 6. This allows a direct measurement of the ratio  $\check{\alpha}/\check{\beta}$  from the experimental distributions which, for run **M** is found to be equal to 0.8, and for run **P** to be of order 4 (see below).

#### 5.5. Comparison for run **P**, the self-similar regime

The experimental distribution  $P(S, n, t)$  for run **P** shows that the conditioned average  $\langle S|n \rangle$  and the variance  $\sigma_n^2$  are proportional to  $n$ , the number of facets. The whole distribution is self-similar in the sense that it depends solely on  $S/\langle S \rangle$ , and  $\langle S \rangle$  scales like time  $t$  (see § 3.1.2).

The occurrence rate of  $\mathcal{T}_2$  processes can be estimated through the statistics of  $\delta n$ . It is found that  $\alpha \approx 3 \text{ h}^{-1}$ , at the first instant and then decays to  $\alpha \approx 0.8 \text{ h}^{-1}$  (figure 16). The direct measurement of the rate of  $\mathcal{T}_1$  processes is unavailable, but the stationary distribution  $P(n, t)$  of the number of facets, which presents an exponential decay, has allowed us to measure, considering that  $\check{\alpha}\mathbb{t} \approx 0.5$ , and using (5.14) in the previous section, the ratio  $\beta/\alpha \approx 1/4$ .

In the limit  $\beta \ll \alpha$ , the expression of  $\bar{\mathcal{Q}}_{\pm}$  simplifies to

$$\bar{\mathcal{Q}}_{\pm} = \frac{2\check{\beta}}{\check{\alpha} + ik} \cdot \frac{1}{\pm 1 + \frac{1}{\tanh((\check{\alpha} + ik)\mathbb{t}/2)}} = \frac{2\check{\beta}}{\check{\alpha} + ik} \cdot \left[ \pm \frac{1}{2} (1 - \exp(\mp(\check{\alpha} + ik)\mathbb{t})) \right] \quad (5.15)$$

showing that  $\mathcal{Q}_+$  is a truncated exponential  $\exp(-\check{\alpha}\mathbb{S})$  between  $\mathbb{S} = 0$  and  $\mathbb{S} = \mathbb{t}$ , and  $\mathcal{Q}_-$  is a truncated exponential between  $\mathbb{S} = -\mathbb{t}$  and  $\mathbb{S} = 0$ ,

$$\mathcal{Q}_{\pm} = \frac{\check{\beta}}{\check{\alpha}} \exp(-\check{\alpha}\mathbb{S}) \cdot \mathbb{1}_{[0, \pm\mathbb{t}]}. \quad (5.16)$$

The distributions  $\mathcal{Q}_{\pm}$  have an average area

$$\langle \mathcal{S}_{\pm} \rangle \approx \pm \mathbb{t} \frac{1 - e^{-\check{\alpha}\mathbb{t}}(1 + \check{\alpha}\mathbb{t})}{\check{\alpha}\mathbb{t}(1 - \exp(-\check{\alpha}\mathbb{t}))}, \quad (5.17a)$$

and variance

$$\sigma_{\mathcal{S}}^2 \approx \mathbb{t}^2 \frac{1 + e^{2\check{\alpha}\mathbb{t}} - e^{\check{\alpha}\mathbb{t}}(2 + (\check{\alpha}\mathbb{t})^2)}{(\check{\alpha}\mathbb{t})^2(-1 + e^{\check{\alpha}\mathbb{t}})^2}, \quad (5.17b)$$

and thus

$$\langle \mathcal{S}_+ \rangle \approx \mathbb{t}/2, \quad \text{for } \check{\alpha}\mathbb{t} \ll 1 \quad \text{and} \quad \langle \mathcal{S}_+ \rangle \propto \check{\alpha}^{-1} \quad \text{for } \check{\alpha}\mathbb{t} \gg 1. \quad (5.18)$$

In the present run  $\mathbf{P}$ ,  $\alpha t$  is nearly constant ( $\alpha t = \check{\alpha}\mathbb{t} \approx 0.5$ ), so that one expects  $\langle \mathcal{S}_+ \rangle \approx 0.4\mathbb{t}$ , and  $\sigma_{\mathcal{S}}^2 \approx 0.08\mathbb{t}^2$ .

The initial condition in run  $\mathbf{P}$  is a mixture of 5-, 6-, and 7-facet cells, and the predicted distribution has the complicated expression

$$P(\mathbb{S}, n, \mathbb{t}) = \sum_{i,j} (\mathcal{A}_{i,j}(\mathbb{S}, n, \mathbb{t}) \otimes \delta(\mathbb{S} + (j-3)\mathbb{t}) \otimes (\mathcal{Q}_- \otimes \mathcal{Q}_+)^{\otimes(i-j)}) \otimes \mathcal{Q}_+^{\otimes n-3}. \quad (5.19)$$

The primary experimental fact that  $\langle S|n \rangle$  and  $\sigma_n^2$  are both proportional to  $n-3$  suggests that  $P(S, n, t)$  is dominated by the  $\mathcal{Q}_+^{\otimes n-3}$  factor, which is close to a Gamma distribution of order  $(n-3)$ , defined by the self-convolution  $(n-3)$  times of an exponential distribution.

The matching is then qualitative, even if the quantitative agreement is weak.

(i) The conditioned mean area is given by  $\langle S|n \rangle = \mathcal{S}_+(n-3) \approx 0.4(n-3)\mathbb{t}$  (5.17a). In dimensional form, this leads to  $\langle S|n \rangle = 0.4(n-3)\dot{S}^*t$ . Numerically,  $\langle S|n \rangle = 38(n-3)t$ , where  $t$  is expressed in hours, and  $S$  in  $\text{mm}^2$ . The measurements reported in figures 7 and 10 (3.7a) show that  $\langle S|n \rangle = 0.35(n-3)\langle S \rangle \approx 30(n-3)t$ .

(ii) The conditioned variance is given by  $\check{\sigma}_n^2 = \sigma_{\mathcal{S}}^2(n-3) \approx 0.08(n-3)\mathbb{t}^2$  (5.17b). In dimensional form, this leads to  $\sigma_n^2 = 0.08(n-3)\dot{S}^{*2}t^2$ . Numerically,  $\sigma_n^2 = 720(n-3)t^2$ , where  $t$  is expressed in hours, and  $\sigma_n^2$  in  $\text{mm}^4$ . The measurements made in figures 7 and 10 (3.7b) show that  $\sigma_n^2 = 0.04(n-3)\langle S \rangle^2 \approx 300(n-3)t^2$ .

The predicted area exceeds by a factor 1.3 the ones that are observed. This disagreement might be due to the contribution of the kernel in (5.19), or to the variation of  $\alpha$  with time (the solution is obtained by assuming  $\alpha$  and  $\beta$  are constants).

The qualitative agreements (on the shapes of the distributions  $P(S, n, t)$  and  $P(n, t)$ ) and the quantitative fits (on the  $n$  dependences of the mean  $\langle S \rangle$  and variances  $\sigma_S^2$ ) suggest that our analysis has captured the main aspects of the coarsening problem, although the temporal dynamic is overestimated.

We explore further the difference between an initially mono- and polydisperse foam, and its relation between the coarsening laws of young and old foams, on hand of an analogy with the Langevin model.

## 6. A Langevin model

The concomitant processes at the origin of the foam ageing are the drift of the cells area according to von Neumann's law (§4.1), and the topological processes  $\mathcal{T}_1$  and  $\mathcal{T}_2$ , (§4.2) which modify their facet number. The 'trajectory' of a cell characteristic (area  $S$ , facet number  $n$ ) has been shown to be ruled by the following set of equations:

$$\left. \begin{aligned} \dot{S} &= \dot{S}^*(n-6), \\ \dot{n} &= -\alpha(n-3) + f(t), \end{aligned} \right\} \quad (6.1)$$

where  $f(t)$  stands for a random process, uncorrelated in time, corresponding to the occurrence of  $\mathcal{T}_1$  processes. Identifying

$$\left. \begin{aligned} S/\dot{S}^* - 3t &\longleftrightarrow x, \\ n - 3 &\longleftrightarrow v, \end{aligned} \right\} \quad (6.2)$$

one sees that it is possible to map the present coarsening problem onto the familiar Langevin process for the dispersion of particles (with position  $x$  and velocity  $v$ ) by thermal agitation (Langevin 1908). The velocity of each particle is damped by viscous drag (whose analogue corresponds to  $\mathcal{T}_2$  processes) with friction coefficient  $\alpha$ , and is randomly altered by the thermal noise of the underlying bath (whose analogue corresponds to  $\mathcal{T}_1$  processes)

$$\left. \begin{aligned} \dot{x} &= v, \\ \dot{v} &= -\alpha v + f(t). \end{aligned} \right\} \quad (6.3)$$

In the simplistic version of the Langevin model, the random noise  $f$  is independent of velocity and position, and is Delta-correlated in time

$$\langle f(t)f(t') \rangle = \epsilon \delta(t-t'). \quad (6.4)$$

This process is well known to give rise to a standard diffusion law for the variance of the particle's positions, which is independent of the initial conditions at large times

$$\sigma_x^2 = \langle x^2 \rangle - \langle x \rangle^2 \sim \frac{\epsilon}{\alpha^2} t \quad \text{for } t \gg 1/\alpha, \quad (6.5)$$

with position  $x$  and velocity  $v$  being correlated according to

$$\langle x|v \rangle \sim \langle x \rangle + v/2\alpha. \quad (6.6)$$

At short times ( $t < 1/\alpha$ ), however, the dispersion law depends on the initial conditions. For particles which are initially all confined at the same location  $x_0$ , and which all have the same initial velocity  $v_0$ , a super-diffusive regime is found (see, e.g. Chapter II.2 in Chandrasekhar 1943)

$$\sigma_x^2 \sim \epsilon t^3, \quad \text{for } t < 1/\alpha, \quad (6.7)$$

$$\langle x|v \rangle \sim \langle x \rangle + (v - v_0)t/2. \quad (6.8)$$

At any time, the distribution of positions and velocities  $P(x, v, t)$  is Gaussian.

Given the formal analogy between the dynamics in (6.1) and (6.3), it is tempting to apply these predictions to the foam problem. However, two major differences exist



between our model of foam ageing and the Langevin model for diffusion, avoiding a strict analogy.

(i) First, the amplitude of the noise is independent of velocity in the Langevin model, whereas the rate of random  $\mathcal{T}_1$  processes is proportional to the number  $(n - 3)$  of cell facets. One may disregard this dependence, and retain the average amplitude only

$$\epsilon \approx \beta \langle n - 3 \rangle = 3\beta \quad (6.9)$$

since  $\langle n \rangle = 6$ .

(ii) Second, the particle velocity is a continuous variable in the Langevin model, whereas the cell number of facets  $n$  is a discrete one.

The consequence of these differences is that  $n$  is exponentially distributed rather than Gaussianly and that  $n$  cannot be smaller than 3 (whereas particle velocities can be positive or negative). However, despite these differences, the scaling laws for the area dispersion remain valid. Runs **M** and **P** thus appear as representative of the two limits recalled above.

(i) Run **M** corresponds to the early super-diffusive regime (characteristic of a young foam), since at initial condition all cells have the same area  $S_0$  and the same number of facets  $n_0 = 6$ . It is therefore expected that the conditioned average of the area is

$$\langle S|n \rangle \sim S_0 + \dot{S}^*(n - 6)t/2, \quad (6.10)$$

which recovers Lewis Law (§3.2), and that the variance (6.7) of the area scales like

$$\sigma_n^2 \sim \beta t^3 \quad (6.11)$$

consistently, taking  $\beta$  as a constant in that case (figure 16), with the experimental observations reported in figure 9. The evolution of the average area  $\langle S \rangle$  is a further consequence of the variance in temporal evolution: the distribution of cell area is a direct consequence of the distribution of facet number ( $\sigma^2 \approx (\dot{S}^*t/2)^2 \langle (n - \langle n \rangle)^2 \rangle \sim t^3$ ). Since the cells' area can only be positive, their average area (which is given by  $\langle S_{rest} \rangle$  in run **M**, itself related to  $S_{cutoff}$ ) grows like  $\sigma \sim t^{3/2}$ , in agreement with the experimental observation in figure 7.

(ii) Run **P** corresponds to the late diffusive regime (characteristic of an old foam) for which the 'particles' are 'thermalized' with a constant distribution of velocity (the distribution of facet  $P(n, t)$  is stationary in the coarsening analogue, as seen in figure 6).

According to (6.5) and (6.9), the typical cell area grows like  $S \sim (3\beta t/\alpha^2)^{1/2}$ . With  $\beta/\alpha$  constant in this case, and  $\alpha$  decreasing like  $1/t$  (see figure 16 and §7.1), one anticipates that

$$S \sim t, \quad (6.12)$$

consistently with what is observed in figure 7.

Note finally that, if we have argued that the dynamics of the cells' area can be viewed as a diffusion process, in which  $S(t)$  experiences a random walk through a Langevin type of mechanism, it is *not* our claim that foam cells diffuse *in the physical space*, with their boundaries fluctuating according to a random walk. This kind of description is made by several authors (Glazier, Anderson & S. 1990; Sire & Majumdar 1995), with q-Potts models in which cells are domains whose borders move according to a random protocol, but this is completely unrelated to our remark here.

## 7. Conclusion and further remarks

The present study has documented experimentally, making use of an original set-up allowing to acquire well-converged data on the coarsening of foams in two dimensions. The experiments have shown that a foam behaves quite differently depending on the way it has been prepared. We have distinguished between an initially quasi-monodisperse foam, and a polydisperse foam. Although both foams reach a common, time-dependent asymptotic regime, the coarsening laws are initially different.

The ageing process relies on exchanges between the foam cells (von Neumann's law), and on topological rearrangement ( $\mathcal{T}_1$  and  $\mathcal{T}_2$  processes) whose rates have been measured in all regimes. We have attempted to make their contribution to the evolution of the area  $S$  and facet number  $n$  distribution of probability  $P(S, n, t)$  quantitative by a mean field theory whose predictions represent well the phenomenon qualitatively, and are sometimes in quantitative agreement with the measurements. A simplified version of this theory, taking the form of a Langevin model, explains in a straightforward manner the different scaling laws in the different regimes, for the different foams.

Critical to the laws of foam coarsening are the rates  $\alpha$  and  $\beta$  of the topological processes  $\mathcal{T}_2$  and  $\mathcal{T}_1$  directing the evolution. It is probably useful at this point to worry about their status, and possible time dependence.

### 7.1. $\mathcal{T}_2$ process and $\alpha$ in the self-similar regime

The process  $\mathcal{T}_2$  corresponds to the disappearance of 3-facet cells, whose area vanish (see §4.1). Run **P** suggests that an estimation of the rate  $\alpha$  is possible in this case. Indeed, a self-similar regime is reached, meaning that the relative proportion of 3-facet cells in the cells assembly is constant. Consequently,

$$\alpha \approx -\frac{1}{N} \frac{dN}{dt}. \quad (7.1)$$

In the self-similar limit, the average area of these 3-facet cells is proportional to  $\langle S \rangle$  itself, so that their lifetime  $1/\alpha$  scales like  $\langle S \rangle / \dot{S}^*$ . Since the total area of the foam is conserved, and that the average area of a single cell increases as a consequence of the disappearance of other cells, one has

$$\frac{1}{\langle S \rangle} \frac{d\langle S \rangle}{dt} = -\frac{1}{N} \frac{dN}{dt} \sim \frac{\dot{S}^*}{\langle S \rangle}, \quad (7.2)$$

showing that  $\langle S \rangle$  is a linear function of time (as shown on figure 6, and demonstrated along similar lines by Glazier & Stavans 1989)

$$\langle S \rangle \sim \dot{S}^* t, \quad (7.3)$$

and also setting the value of  $\alpha$

$$\alpha \sim 1/t. \quad (7.4)$$

The distribution  $P(S, n, t)$  is fixed by the shape of the kernel  $\mathcal{Q}_+^{\otimes n-3}$  whose shape depends only on  $\alpha t$  (when  $\beta \ll \alpha$ , see (5.15)). The fact that  $\alpha t$  tends toward a constant is an *a posteriori* justification of the self-similar behaviour of  $P(S, n, t)$ .

Note that this self-similar regime is not a steady-state regime, and that this is therefore not an equilibrium regime. The parameter ruling the foam evolution is not  $t$ , but  $\alpha t$ . Since the rates  $\alpha$  and  $\beta$  decrease (at least in run **P**) in time like  $1/t$ ,  $\alpha t$  is not likely to attain very large values, so that the true equilibrium, diffusional self-similar regime in the sense of our Langevin model, is in fact never completely reached. A

foam is, for most of its lifetime, experiencing a transient regime. Thermodynamical considerations on the maximization of a foam entropy lead Iglesias & de Almeida (1991) to predict an equilibrium distribution  $P(S, n, t)$ , which is thus not likely to describe the present experiments.

### 7.2. $\mathcal{T}_1$ process and $\beta$

A foam rearranges through  $\mathcal{T}_1$  processes to relax internal stresses with a characteristic time that itself is a function of the intensity of the residual stress (Gopal & Durian 1995; Cohen-Addad & Hohler 2001). The rearrangement dynamics is thus slowing down in time. It is, to this respect, not surprising that  $\beta$ , the rate of  $\mathcal{T}_1$  processes, is found to decay in time in the self-similar regime of old foams, as is  $\alpha$ . It is on the other hand found to be roughly constant in young foams, those where coexist clusters of perfect hexagonal cells (the ‘stock cells reservoirs’), and regions of ageing foam, surrounding them. This coexistence may be at the origin of the ever-renewed stress making  $\beta$  constant.

In the Langevin analogue to the coarsening problem derived in §6,  $\beta$  is a measure of the agitation of the medium, setting an apparent temperature to the system. A perfect hexagonal lattice is at zero temperature, since no topological process occurs. The disorder imposed by the rearrangements in the foam, or by an external strain increases the temperature; but it is at this point difficult to make a precise description of it, and in any case out of the scope of the present paper.

Finally, we note that a self-similar regime is also observed for three-dimensional ageing foams, leading to a lognormal distribution of the face number and an exponential distribution of the cell volumes (Lambert *et al.* 2009). Although there is no strict equivalent of von Neumann’s law in three-dimensional foams (Monnereau & Vignes-Adler 1998; Hilgenfeldt *et al.* 2001; Hilgenfeldt 2002; Streitenberger & Zollner 2006; MacPherson & Srolovitz 2007), a mean field formulation of the kind of equation (5.2) with cell population averaged, effective rates for the disappearance of the smallest cells and the change of cells’ facets numbers, is likely to be even more justified compared to the two-dimensional case: a cell neighbourhood will explore even more completely the average medium statistics in three than in two dimensions.

This work has been supported by the Agence Nationale de la Recherche (ANR) through grant ANR-05-BLAN-0222-01. Comments and suggestions by I. Cantat and S. Hilgenfeldt have been helpful.

## Appendix A. The von Neumann’s Law

The growth of cells’ area  $dS/dt$  is linked, in two dimensions, to their facet number  $n$ , and von Neumann (1952) showed that,

$$\frac{dS}{dt} = \dot{S}^*(n - 6), \quad (\text{A } 1)$$

with

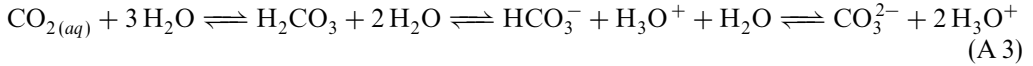
$$\dot{S}^* = \frac{4\pi}{6} \gamma \frac{DC^*}{h} V_M, \quad (\text{A } 2)$$

with  $\gamma$  the liquid surface tension,  $D$  the diffusivity coefficient of the dissolved species in the liquid constitutive of the foam,  $C^*$  the solubility concentration of the species involved in mass transport through the separatrix,  $h$  the cell separatrix wall thickness and  $V_M$  the molar volume of the gas. Figure 12 shows the linear relationship between  $n$  and  $dS/dt$ , from which  $\dot{S}^*$  has been measured.

This allows an indirect measurement of the wall thickness  $h$ , which is found to be of the order of 40 nm (run **M**) and 60 nm (run **P**) with  $D = 1.9 \times 10^{-9} \text{ m}^2 \text{ s}^{-1}$  for  $\text{CO}_2$  in water. These values are independent of the age of the foam, excluding the influence of drainage on the ageing dynamics. The maximal age of the foam is about 2 h (for run **M**), whereas Glazier & Stavans (1989) report an effect of drainage on the ageing dynamics for experiments lasting typically over 100 h.

The von Neumann's relationship (4.1) holds under certain assumptions as follows.

(i) When  $\text{CO}_2$  dissolves in water, it forms a hydrated complex  $\text{H}_2\text{CO}_3$ . The latter reacts and acidifies water:



and forms bicarbonate ions. At the experimental pH condition (pH = 8.6), the dominant form is  $\text{HCO}_3^-$ , which is in fast equilibrium with  $\text{H}_2\text{CO}_3$  and  $\text{CO}_3^{2-}$ , but in slow equilibrium with  $\text{CO}_{2(aq)}$ . One gets, at equilibrium

$$\left. \begin{aligned} [\text{CO}_{2(aq)}]_{eq} &= P_{\text{CO}_2} [\text{H}_2\text{O}] / K_H, \\ [\text{H}_2\text{CO}_3]_{eq} &= [\text{CO}_{2(aq)}]_{eq} / K_D, \\ [\text{HCO}_3^-]_{eq} &= [\text{CO}_{2(aq)}]_{eq} 10^{\text{pH} - pK_{a1}} = [\text{CO}_{2(aq)}]_{eq} / K, \\ [\text{CO}_3^{2-}]_{eq} &= [\text{CO}_{2(aq)}]_{eq} 10^{2\text{pH} - pK_{a1} - pK_{a2}}, \end{aligned} \right\} \quad (\text{A } 4)$$

where  $K_H = 163 \text{ MPa}$  denotes the Henry pressure,  $K_D \approx 650$  denotes the dissociation constant of hydration reaction and  $pK_{a1} = 6.35$  and  $pK_{a2} = 10.33$  the dissociation constant of acidobasic reactions (note that the dissociation constants of the acidobasic reaction  $K_{a1}$  and  $K_{a2}$  are reported with respect to  $\text{CO}_{2(aq)}$ ). The pressure drop from one side to the other of the separatrix (in the direction  $x$ ) imposes a concentration gradient  $\partial_x[\cdot]$  for all species. Accounting for the kinetic of these reactions, the concentration profile in a separatrix is driven by the following set of reaction–diffusion equations:

$$\left. \begin{aligned} \partial_t [\text{CO}_{2(aq)}] &= D \partial_x^2 [\text{CO}_{2(aq)}] - k_+ [\text{CO}_{2(aq)}] + k_- [\text{H}_2\text{CO}_3], \\ \partial_t [\text{H}_2\text{CO}_3] &= D \partial_x^2 [\text{H}_2\text{CO}_3] + k_+ [\text{CO}_{2(aq)}] - (k_- + K_+) - K_- [\text{H}_2\text{CO}_3] \\ &\quad + [\text{HCO}_3^-] [\text{H}_3\text{O}^+], \\ \partial_t [\text{HCO}_3^-] &= D \partial_x^2 [\text{HCO}_3^-] + K_+ [\text{H}_2\text{CO}_3] - K_- [\text{HCO}_3^-] [\text{H}_3\text{O}^+], \end{aligned} \right\} \quad (\text{A } 5)$$

where the diffusivity  $D$  of all species is assumed to be identical,  $k_+$ ,  $k_-$  are the hydration reaction rates and  $K_+$  and  $K_-$  are the acidobasic reaction rates. For simplicity, we did not consider the production of  $\text{CO}_3^{2-}$ , which exists in negligible amount. Considering that the acidobasic reaction is fast with respect to the hydration reaction,  $\text{H}_2\text{CO}_3$  and  $\text{HCO}_3^-$  are in equilibrium

$$[\text{HCO}_3^-] = [\text{H}_2\text{CO}_3] \frac{K_D}{K}, \quad (\text{A } 6)$$

where  $K = 10^{\text{pH} - pK_{a1}}$ . The system reduces to

$$\left. \begin{aligned} \partial_t [\text{CO}_{2(aq)}] &= D \partial_x^2 [\text{CO}_{2(aq)}] - k_+ [\text{CO}_{2(aq)}] + k_- \frac{K}{K_D} [\text{HCO}_3^-], \\ \partial_t [\text{HCO}_3^-] &= D \partial_x^2 [\text{HCO}_3^-] + \left( k_+ [\text{CO}_{2(aq)}] - k_- \frac{K}{K_D} [\text{HCO}_3^-] \right) / (1 + K/K_D). \end{aligned} \right\} \quad (\text{A } 7)$$

At the interfaces ( $x = -h/2$  and  $x = +h/2$ ), the dissolution kinetic might be considered as infinitely rapid and the concentration of  $\text{CO}_{2(aq)}$  is fixed by the pressure

$$[\text{CO}_{2(aq)}] \Big|_{\pm h/2} = P_{\pm} [\text{H}_2\text{O}] / K_H. \quad (\text{A } 8)$$

The concentration gradient of  $\text{H}_2\text{CO}_3$  and  $\text{HCO}_3^-$  vanishes as these molecules might not be transferred to the gas phase. Considering finally the stationary state, we get (with  $K/K_D \ll 1$ ) the following concentration profile:

$$\left. \begin{aligned} [\text{CO}_{2(aq)}] &= [\text{CO}_{2(aq)}]_{eq} + \frac{1}{\mathcal{K}} (Ak_-x + B \sinh(\sqrt{\mathcal{K}/D}x)), \\ [\text{HCO}_3^-] &= [\text{HCO}_3^-]_{eq} + \frac{1}{\mathcal{K}} (Ak_+x - B \sinh(\sqrt{\mathcal{K}/D}x)), \\ A &= \frac{\Delta P [\text{H}_2\text{O}]}{2K_h} \mathcal{K} \left[ \frac{K}{K_D} k_- \frac{h}{2} + k_+ \sqrt{\frac{D}{\mathcal{K}}} \tanh\left(\sqrt{\frac{\mathcal{K}h}{D}}\right) \right]^{-1}, \\ B &= k_+ A / \sqrt{\frac{\mathcal{K}}{D}} \cosh\left(\sqrt{\frac{\mathcal{K}h}{D}}\right), \\ \mathcal{K} &= k_+ + k_- \frac{K}{K_D}, \end{aligned} \right\} \quad (\text{A } 9)$$

and the mass flux density is

$$\phi = D \frac{\Delta P}{K_H h} \left( \frac{k_+ + k_- K/K_D}{k_+ \frac{\tanh(\sqrt{\mathcal{K}h^2/4D})}{\sqrt{\mathcal{K}h^2/4D}} + k_- K/K_D} \right), \quad (\text{A } 10)$$

where the contribution of  $\text{H}_2\text{CO}_3$  and  $\text{CO}_3^{2-}$  ions has been neglected. However, the kinetic of the acidobasic reaction is slow compared to the diffusion time (Soli & Byrne 2002 report a reaction time  $\tau_R \sim 1/(k_+ + k_- K/K_D) \approx 30$  s), a time much larger than the diffusion time through the separatrix. Thus, the concentration profile  $[\text{HCO}_3^-]$  is homogeneous across the separatrix thickness, and only  $\text{CO}_{2(aq)}$  contributes to the transport of carbon dioxide through the wall. Finally,

$$C^* = [\text{H}_2\text{O}]/K_H. \quad (\text{A } 11)$$

(ii) The angle between two consecutive borders should be exactly  $2\pi/3$ . This angle corresponds to the mechanical equilibrium at the vertex point, where three cell borders join. The lack of resolution of our images prevents the accurate measurement of this angle. Stavans & Glazier (1989) measured a small correction due to nonlinear bending effect of the Plateau border. This correction induces to a stronger curvature for small cells (with  $n \leq 6$ ), and is expected to cause a mass over-flux of 50 % for 3-sided cells. This effect is not seen on our measurements of the average of  $\delta S_n$ .

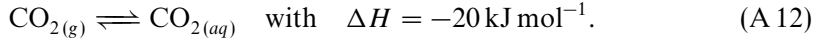
(iii) The foam should be really two-dimensional. The von Neumann relation links mass flux to facets number  $n$ . The thickness variation of separatrix should be taken into account, if not constant. This variation is confined into tiny Plateau borders whose influence on the global mass exchanges is negligible, even for the smallest cells.

(iv) The Fick flux is estimated in the stationary limit. The transient lasts for  $h^2/D \approx 2.5 \mu\text{s}$  and is negligible since it is infinitely short compared to the evolution times discussed here (hours).

(v) The vapour should be composed of one single gas (so that chemical and mechanical equilibrium are related to one unique pressure). We work with  $\text{CO}_2$  around atmosphere, so that the contribution of water vapour (whose partial pressure is  $P_{sat} = 30$  mbar at ambient temperature) is negligible.

(vi) The characteristic flux  $\dot{S}^*$  depends on the solubility of the gas in the liquid, which is sensitive to temperature. The foam should then be isotherm. The dissolution

of  $\text{CO}_2$  is exothermic



The mass flux is of order

$$\phi \sim \frac{4\pi DC^* \gamma}{6 h \mathcal{P}}, \quad (\text{A } 13)$$

where  $\mathcal{P}$  is the typical cell perimeter. We find  $\phi \approx 2 \times 10^{-4} \text{ mol m}^{-2} \text{ s}^{-1}$  here typically. The corresponding reaction rate induces a variation of temperature of about  $10^{-8} \text{ K}$ , which is clearly negligible.

## Appendix B. Solution of the model

We present an analytic solution of (5.2) for the particular initial condition corresponding to run *M*. The generalization to any initial condition is possible, making use of the linearity of (5.2).

### B.1. Transformation

Equation (5.2) is a second-order partial derivative equation, along variable time  $t$ , area  $S$  and a discrete derivation on the number of facets  $n$ . A transformation of this equation in Fourier space  $(t, k, q)$ , where  $k$  and  $q$  are the dual variable for  $S$  and  $n$ , respectively simplifies the problem. Define

$$\tilde{P}(k, q, t) = \int dS dn \exp(-ikS - iq[n-3])P(S, n, t), \quad (\text{B } 1)$$

where the integration extends from negative to positive area and facet number, and  $n$  is a continuous variable; (5.2) becomes

$$\partial_t \tilde{P} = 3ik\tilde{P} + k\partial_q \tilde{P} + \alpha i(e^{iq} - 1)\partial_q \tilde{P} + \beta 2i(\cos(q) - 1)\partial_q \tilde{P}, \quad (\text{B } 2)$$

which is a first-order partial derivative, linear equation along two variables  $t$  and  $q$ . A further transformation

$$\left. \begin{aligned} t' &= t - \frac{2 \arctan\left(\frac{-\alpha - 2\beta + 2(\alpha + \beta)e^{iq} - ik}{\sqrt{-\alpha^2 - 2i\alpha k + k(-4i\beta + k)}}\right)}{\sqrt{-\alpha^2 - 2i\alpha k + k(-4i\beta + k)}}, \\ k' &= k, \\ q' &= q, \end{aligned} \right\} \quad (\text{B } 3)$$

such that

$$\left. \begin{aligned} \partial_t &= \partial_{t'}, \\ \partial_q &= \partial_{q'} + \frac{1}{k + i\alpha(e^{iq} - 1) + 2i\beta(\cos(q) - 1)} \partial_{t'}, \end{aligned} \right\} \quad (\text{B } 4)$$

leads to a first-order ordinary differential equation

$$3ik'P' + (k' + i\alpha(e^{-iq'} - 1) + 2i\beta(\cos(q') - 1))\partial_{q'}P' = 0. \quad (\text{B } 5)$$

### B.2. Solution

The solution of (B 5) is of the form

$$\ln(P') = \frac{6i k'}{\sqrt{-\alpha^2 - 2i(\alpha + 2\beta)k' + k'^2}} \arctan\left(\frac{-\alpha - 2\beta + 2(\alpha + \beta)e^{iq'} - ik'}{\sqrt{-\alpha^2 - 2i(\alpha + 2\beta)k' + k'^2}}\right) + f(k', t'), \quad (\text{B } 6)$$

where  $f(k', t')$  is some function which must match the initial condition. For the case of run  $M$ , the initial area distribution is a Dirac delta at  $S = S_0$ , and all cells have all  $n_0 = 6$  facets

$$P(S, n, t = 0) = \delta(S - S_0)\delta_{n, n_0}, \quad (\text{B } 7)$$

so that

$$\ln(\tilde{P}(k, q, t = 0)) = -ikS_0 - (n_0 - 3)iq, \quad (\text{B } 8)$$

which imposes that

$$\begin{aligned} f(k', t') = & -ik'S_0 + 3ik't' \\ & - (n_0 - 3) \ln \left[ -\frac{\sqrt{-\alpha^2 - 2i\alpha k' + k'(-4i\beta + k')}}{2(\alpha + \beta)} \right. \\ & \left. \times \left( \tan \left[ \frac{\sqrt{-\alpha^2 - 2i\alpha k' + k'(-4i\beta + k')t'}}{2} \right] \right) + \frac{\alpha + ik + 2\beta}{2(\alpha + \beta)} \right], \end{aligned} \quad (\text{B } 9)$$

and one gets

$$\tilde{P}(k, q, t) = \exp(ikS_0 - i3kt)\tilde{K}(k, q, t)^{-(n_0-3)}, \quad (\text{B } 10)$$

where

$$\begin{aligned} \tilde{K}(k, q, t) = & \frac{\alpha + ik + 2\beta}{2(\alpha + \beta)} \\ & - \frac{\sqrt{-\alpha^2 - 2i\alpha k + k(-4i\beta + k)}}{2(\alpha + \beta)} \left( \tan \left[ \frac{\sqrt{-\alpha^2 - 2i\alpha k + k(-4i\beta + k)t}}{2} \right] \right. \\ & \left. - \arctan \left( \frac{-\alpha - 2\beta + 2(\alpha + \beta)e^{iq} - ik}{\sqrt{-\alpha^2 - 2i\alpha k + k(-4i\beta + k)}} \right) \right). \end{aligned} \quad (\text{B } 11)$$

Finally, it is possible to perform the inverse Fourier transform of the kernel  $\tilde{K}(k, q, t)$  along the variables  $(n, q)$

$$\bar{K}(k, n, t) = \bar{\varrho}_-^{-1} \left( \delta(n - 3) + \left[ -1 + \frac{\alpha + \beta}{\beta} \bar{\varrho}_+ \bar{\varrho}_- \right] \bar{\varrho}_+^{n-3} \right), \quad \text{for } n \in \mathbb{N}. \quad (\text{B } 12)$$

In order to obtain  $\bar{P}(k, n, t)$ , the kernel  $\bar{K}$  has to be convoluted  $n_0 - 3$  times, with respect to  $n$ ,

$$\begin{aligned} \bar{P}(k, n, t) = & \exp(ikS_0 - i3kt)\bar{\varrho}_-^{-(n_0-3)} \left[ \delta_{n,0} + \left( \sum_{i=1}^{n_0-3} C_{n_0-3}^i C_{n-3+i-1}^{i-1} \right. \right. \\ & \left. \left. \times \left[ -1 + \frac{\alpha + \beta}{\beta} \bar{\varrho}_+ \bar{\varrho}_- \right]^i \right) \bar{\varrho}_+^{n-3} \right], \end{aligned} \quad (\text{B } 13)$$

which can be rewritten as

$$\bar{P}(k, n, t) = \exp(ikS_0 - i3kt)\bar{\varrho}_-^{-(n_0-3)} \left( \sum_{i=0}^{n_0-3} C_{n_0-3}^i C_{n-3+i-1}^{n_0-3-1} \left[ -\frac{\alpha + \beta}{\beta} \bar{\varrho}_+ \bar{\varrho}_- \right]^i \right) \bar{\varrho}_+^{n-3}. \quad (\text{B } 14)$$

## REFERENCES

- ABOAV, D. A. 1980 The arrangement of cells in a net. *Metallography* **13**, 43–58.
- BEENAKKER, C. W. J. 1986 Evolution of two-dimensional soap-film networks. *Phys. Rev. Lett.* **57** (19), 2454–2457.
- BOHN, S., DOUADY, S. & COUDER, Y. 2005 Four sided domains in hierarchical space dividing patterns. *Phys. Rev. Lett.* **94**, 054503.
- CANTAT, I., KERN, N. & DELANNAY, R. 2004 Dissipation in foam flowing through narrow channels. *Europhys. Lett.* **65** (5), 726–732.
- CHANDRASEKHAR, S. 1943 Stochastic problems in physics and astronomy. *Rev. Mod. Phys.* **15** (1), 1–89.
- CLERI, F. 2000 A stochastic grain growth model based on a variational principle for dissipative systems. *Physica A* **282**, 339–354.
- COHEN-ADDAD, S. & HOHLER, R. 2001 Bubble dynamics relaxation in aqueous foam probed by multispeckle diffusing-wave spectroscopy. *Phys. Rev. Lett.* **86** (20), 4700–4703.
- DURAND, M. & STONE, H. A. 2006 Relaxation time of the topological t1 process in a two-dimensional foam. *Phys. Rev. Lett.* **97**, 226101.
- FLYVBJERG, H. 1993 Model for coarsening froths and foams. *Phys. Rev. E* **47** (6), 4037–4054.
- GLAZIER, J. A., ANDERSON, M. P. & GREST, G. S. 1990 Coarsening in the two-dimensional soap froth and the large-q Potts model: a detailed comparison. *Phil. Mag. B* **62** (6), 615–645.
- GLAZIER, J. A., GROSS, S. P. & STAVANS, J. 1987 Dynamics of two-dimensional soap froths. *Phys. Rev. A* **36** (1), 306–312.
- GLAZIER, J. A. & STAVANS, J. 1989 Non-ideal effects in the two-dimensional soap froth. *Phys. Rev. A* **40** (12), 7398–7401.
- GOPAL, A. D. & DURIAN, D. J. 1995 Nonlinear bubble dynamics in a slowly driven foam. *Phys. Rev. Lett.* **75** (13), 2610–2613.
- HANSEN, F. K. & RODSRUD, G. 1991 Surface tension by pendant drop. *J. Colloid Interface Sci.* **141** (1), 1–9.
- HILGENFELDT, S. 2002 Bubble geometry. *Nieuw Archief voor Wiskunde* **5** (3), 224–230.
- HILGENFELDT, S., ARIF, S. & TSAI, J.-C. 2008 Foam: a multiphase system with many facets. *Phil. Trans. A* **366**, 2145–2159.
- HILGENFELDT, S., KRAYNIK, A. M., KOEHLER, S. A. & STONE, H. A. 2001 An accurate von Neumann's law for three-dimensional foams. *Phys. Rev. Lett.* **86**, 2685–2688.
- DE ICAZA, M., JIMENEZ CENICEROS, A. & CASTANO, V. M. 1994 Statistical distribution functions in 2d foams. *J. Appl. Phys.* **76**, 7317–7322.
- IGLESIAS, J. R. & DE ALMEIDA, R. M. C. 1991 Statistical thermodynamics of a two-dimensional cellular system. *Phys. Rev. A* **43** (6), 2763–2770.
- KRICHEVSKY, O. & STAVANS, J. 1992 Coarsening of two-dimensional soap froths in the presence of pinning centers. *Phys. Rev. B* **46** (17), 10579–10582.
- LAMBERT, J., MOKSO, R., CANTAT, I., CLOETENS, P., GLAZIER, J. A., GRANER, F. & DELANNAY, R. 2009 Coarsening foams robustly reach a self-similar growth regime. *Phys. Rev. Lett.* **104**, 248304.
- LANGEVIN, P. 1908 Sur la théorie du mouvement Brownien. *Comptes Rendus Acad. Sci. Paris* **146**, 530–533.
- LEVITAN, B., SLEPYAN, E., KRICHEVSKY, O., STAVANS, J. & DOMANY, E. 1994 Topological distribution of survivors in an evolving structure. *Phys. Rev. Lett.* **73** (5), 756–759.
- LEWIS, F. T. 1928 The correlation between cell division and the shapes and sizes of prismatic cells in the epidermis of cucumis. *Anat. Rec.* **38** (3), 341–376.
- MACPHERSON, R. D. & SROLOVITZ, D. J. 2007 The von Neumann relation generalized to coarsening of three-dimensional microstructures. *Nature* **446**, 1053–1055.
- MARDER, M. 1987 Soap-bubble growth. *Phys. Rev. A* **36** (1), 438–440.
- MIRI, M. & RIVIER, N. 2006 Universality in two-dimensional cellular structures evolving by cell division and disappearance. *Phys. Rev. E* **73** (3), 031101.
- MOMBACH, J. C. M., DE ALMEIDA, R. M. C. & IGLESIAS, J. R. 1993 Mitosis and growth in biological tissues. *Phys. Rev. E* **48** (1), 598–602.
- MONNEREAU, C. & VIGNES-ADLER, M. 1998 Dynamics of 3d real foam coarsening. *Phys. Rev. Lett.* **80** (23), 5228–5231.
- VON NEUMANN, J. 1952 Discussion. *Metal Interfaces*, pp. 108–110. American Society of Metals.



- PRODI, F. & LEVI, L. 1980 Aging of accreted ice. *J. Atmos. Sci.* **37**, 1375–1384.
- SEGEL, D., MUKAMEL, D., KRICHEVSKY, O. & STAVANS, J. 1993 Selection mechanism and area distribution in two-dimensional cellular structures. *Phys. Rev. E* **47** (2), 812–819.
- SIRE, C. & MAJUMDAR, S. N. 1995 Correlations and coarsening in the  $q$ -state Potts model. *Phys. Rev. Lett.* **74** (21), 4321–4324.
- SOLI, A. L. & BYRNE, R. H. 2002 CO<sub>2</sub> system hydration and dehydration kinetics and the equilibrium CO<sub>2</sub>/H<sub>2</sub>CO<sub>3</sub> ratio in aqueous NaCl solution. *Mar. Chem.* **78**, 65–73.
- STAVANS, J. 1990 Temporal evolution of two-dimensional drained soap froths. *Phys. Rev. A* **42** (8), 5049–5051.
- STAVANS, J. 1993 The evolution of cellular structures. *Rep. Prog. Phys.* **56**, 733–789.
- STAVANS, J. & GLAZIER, J. A. 1989 Soap froth revisited: dynamic scaling in the two-dimensional froth. *Phys. Rev. Lett.* **62** (11), 1318–1321.
- STREITENBERGER, P. & ZOLLNER, D. 2006 Effective growth law from three-dimensional grain growth simulations and new analytical grain size distribution. *Scr. Mater.* **55**, 461–464.
- SZETO, K. Y., ASTE, T. & TAM, W. Y. 1998 Topological correlations in soap froths. *Phys. Rev. E* **58** (2), 2656–2659.
- SZETO, K. Y. & TAM, W. Y. 1995 Lewis' law versus Feltham's law in soap froth. *Physica A: Stat. Theor. Phys.* **221** (1–3), 256–262, Proceedings of the Second IUPAP Topical Conference and the Third Taipei International Symposium on Statistical Physics.
- TAM, W. Y. & SZETO, K. Y. 1996 Evolution of soap froth under temperature effects. *Phys. Rev. E* **53** (1), 877–880.
- WEAIRE, D. & HUTZLER, S. 1999 *The Physics of Foams*. Oxford University Press.